NASA Technical Paper 2292

March 1984

Generalization of the Subsonic Kernel Function in the s-Plane, With Applications to Flutter Analysis

Herbert J. Cunningham
and Robert N. Desmarais

NASA

NASA
Technical
Paper
2292

1984

Generalization of the Subsonic Kernel Function in the s-Plane, With Applications to Flutter Analysis

Herbert J. Cunningham
and Robert N. Desmarais

Langley Research Center
Hampton, Virginia

NASA
National Aeronautics
and Space Administration

Scientific and Technical
Information Branch

SUMMARY

A generalized subsonic unsteady aerodynamic kernel function, valid for both growing and decaying oscillatory motions, is developed and applied in a modified flutter analysis computer program to solve for boundaries of constant damping ratio as well as the flutter boundary. Results are given for the variation of generalized aerodynamic forces with the damping ratio. Some comparisons are made with an alternative method of obtaining generalized forces based on rational function approximations of simple harmonic forces. For decaying motion, instances were observed of unexpected looping and spiraling of generalized aerodynamic forces calculated in the complex plane at high reduced frequencies. Similar spiraling behavior was found for two-dimensional flow for which convergence of the results with respect to downwash collocation was proven. Rates of change of damping ratios with respect to dynamic pressure near flutter are substantially lower from the generalized-kernel-function calculations than from the conventional velocity-damping (V-g) calculation. For the DAST ARW-1[1], calculated values of both damping ratios and frequencies agreed with the in-flight experimental values for Mach numbers approaching the flutter condition. The aerodynamic forces from the rational function approximation used in control theory for s-plane analysis agreed fairly well with kernel-function results except for strongly damped motion at combinations of high (subsonic) Mach number and reduced frequency.

INTRODUCTION

Considerable flutter analysis has been accomplished using the subsonic kernel function that originated from the lifting-surface-theory work of H. G. Küssner (1940) that is based on the linear theory of potential flow. Watkins, Runyan, and Woolston (1955) cast the kernel function in a form amenable to automated computation. The function was developed by assuming simple harmonic (i.e., constant-amplitude) motion that had continued for an infinite time. Thus, in a flutter analysis the resulting aerodynamic forces are valid only at the flutter boundary, but are not strictly valid for growing or decaying motion at speeds above and below a flutter boundary.

Numerous analyses have attempted to forecast the near-flutter and approach-to-flutter behavior of lifting surfaces. Such efforts began at least as early as the velocity-damping (V-g) solutions of Smilg and Wasserman (1942) and continue today in the rational function approximation (RFA) described by Sevart (1975) and applied, for example, by Abel (1979).

The present report generalizes the subsonic kernel function into the s-plane for arbitrary values of the complex reduced frequency. This kernel function is then applied to analyze the near-flutter behavior of several configurations using the equations of dynamic equilibrium of Cunningham (1978). The calculations were carried out by a modified version of the flutter analysis computer programs described by Desmarais and Bennett (1978). An appendix describes the evaluation of the kernel function by an accurate series approximation for which the computation is economical.

---

[1]Drones for Aerodynamic and Structural Testing (DAST), aeroelastic research wing 1 (ARW-1).

The present results are compared with both the near-flutter results from the V-g method and the results from RFA aerodynamics in control theory.

SYMBOLS

a_s speed of sound

$\bar{A}_{ij}$ generalized aerodynamic force, equation (5)

A_n coefficients of the rational function approximation (RFA), equation (6)

b_o root semichord, often reference length

C_{L_α} lift-curve slope

ΔC_{p_j} lifting pressure coefficient for unit amplitude of mode j, $\Delta p_j/(\rho V^2/2)$

f cyclic frequency of motion

g_i mechanical hysteresis structural damping coefficient of mode i

g root-finding increment added to g_i

$h_i(x,y)$ mode shape of mode i

i imaginary unit, $\sqrt{-1}$

$\mathrm{Im}(\ )$ imaginary part of $(\ )$

k reduced frequency, $\frac{\omega b_o}{V}$ and $\frac{\omega \ell}{V}$

k_c complex reduced frequency, $k(1 + i\bar{\zeta})$

$K(M,k,x_o,y_o)$ generalized kernel function for real k and for k replaced by $k(1 + i\bar{\zeta})$

$\bar{K}(M,k,x_o,y_o)$ kernel function with singular factor removed, equation (3)

ℓ reference length, optionally equal to b_o

m_i generalized mass for mode i

M Mach number of undisturbed stream

N number of modes in analysis

$\Delta p(x,y,t)$ lifting pressure distribution

Δp_j $= \partial(\Delta p)/\partial(q_j/\ell)$

$q_i(t)$	generalized coordinate of mode i
$\hat{Q}$	rational function approximation for any $\bar{A}_{ij}$, equation (6)
r	$\beta\sqrt{y_o^2 + z^2}$
R	$\sqrt{x_o^2 + \beta^2 y_o^2}$
Re( )	real part of ( )
RFA	rational function approximation
s	$= i\omega(1 + i\bar{\zeta})$, coefficient of t for general exponential time-varying motion e^{st}; also the Laplace transform variable
$\bar{s}$	$= s\ell/V$
S	planform area of lifting surface
t	time
u_1	$= \left(-x_o + MR\right)/\left(\beta^2\lvert y_o\rvert\right)$
V	speed of undisturbed flow
$w(x,y,t)$	downwash distribution, positive with z
x,y,z	orthogonal, right-handed coordinates nondimensionalized by ℓ, x positive downstream, y positive on the right-hand half-span, z positive up
x_o	$= x - \xi$
y_o	$= y - \eta$
α	angle of attack, pitch displacement
β	$= \sqrt{1 - M^2}$
β_n	aerodynamic lag parameters in equation (6)
δ	logarithmic decrement of oscillatory motion, positive for decay
ζ	damping ratio of control theory, $\cos\theta$
$\bar{\zeta}$	damping ratio used herein, defined in equation (9)
η	dummy variable for y
θ	angle from negative real s-axis to s of motion (see sketch on p. 5)
μ	mass ratio, wing mass divided by the mass of air in a truncated cylindrical cone that just encloses the wing planform
ξ	dummy variable for x

ρ air density

ω circular frequency of motion, radians/sec

ω_i natural frequency of mode i

ω_o base or reference frequency, equations (4)

ω_α natural frequency of torsion mode

ANALYSIS

Downwash Integral Equation and Kernel Function

The phenomenon studied here is that of a thin lifting surface oscillating normal to the direction of a compressible flow. The linear, small disturbance equations of potential flow along with the associated boundary conditions are used to analyze this phenomenon.

Based on the pioneer work of Küssner (1940), the integral equation that relates downwash and lifting pressure difference on a planar lifting surface can be put in the form

$$\frac{-w(x,y,t)}{V} = \frac{1}{4\pi\rho V^2} \int\int_S \Delta p(\xi,\eta,t)\ K(M,k,x_o,y_o)\ d(\ell\xi)\ d(\ell\eta) \tag{1}$$

where $K(M,k,x_o,y_o)$ is the kernel function relating the downwash produced at x,y due to unit lifting pressure at ξ,η.

Watkins, Runyan, and Woolston (1955) expressed the subsonic planar ($z = 0$) kernel function as

$$K(M,k,x_o,y_o) = \lim_{z\to 0} \frac{\partial^2}{\partial(\ell z)^2} \left\{ \exp(-ikx_o) \int_{-\infty}^{x_o} \frac{\exp\left[ik\left(\lambda - M\sqrt{\lambda^2 + r^2}\right)/\beta^2\right]}{\sqrt{\lambda^2 + r^2}}\, d\lambda \right\} \tag{2}$$

where λ, the streamwise variable of integration for $x - \xi$, is positive downstream. The integral in equation (2) sums up the effects on the downwash at x,y at the present instant of all pressure disturbances which originated at ξ,η over all past time.

Carrying out the differentiation of equation (2), taking the limit, and integrating by parts changes the form of the planar kernel function to

$$K = \frac{1}{\ell^2 y_o^2}\, \bar{K}$$

where

$$\bar{K}(M,k,x_o,y_o) = \exp(-ikx_o)\left[\left(1 + \frac{x_o}{R}\right)\exp\left(-iku_1|y_o|\right)\right.$$

$$\left. - ik|y_o|\int_{u_1}^{\infty}\left(1 - \frac{u}{\sqrt{1+u^2}}\right)\exp\left(-ik|y_o|u\right)\,du\right] \qquad (3)$$

The calculation of $\bar{K}$ is described in the appendix.

Consider now the generalization from simple harmonic (constant-amplitude) motion with time variation exp iωt (real ω) to growing and decaying oscillatory motion with time variation exp st (complex s). Such motions have come to be termed "s-plane motions," where in the complex s-plane, $s = i\omega$ is the positive imaginary axis. As indicated in the accompanying sketch, for growing motion the real part of s is positive and for decaying motion the real part of s is negative.

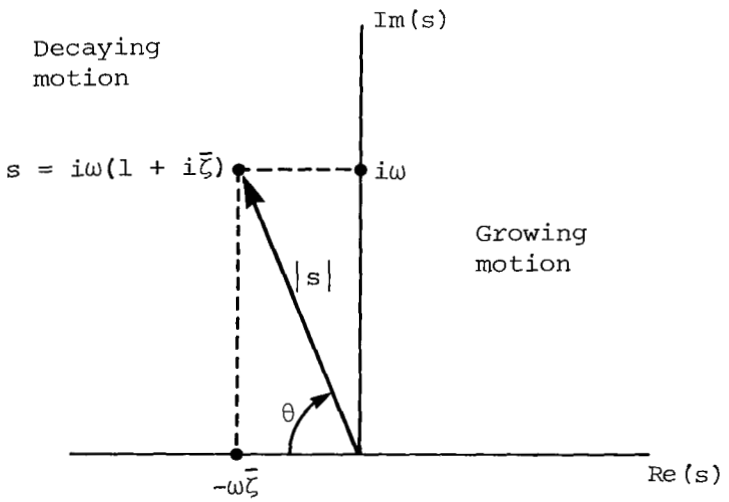

The generalization to growing and decaying motion from harmonic motion is accomplished by replacing the frequency ω by $\omega(1 + i\bar{\zeta})$, where $\bar{\zeta}$ is a motion damping ratio that is positive for decay. The parameter $\bar{\zeta} = \delta/2\pi$, where δ is the logarithmic decrement of motion, as described, for example, in Cunningham (1978). The sketch shows that this definition of the damping ratio is equivalent to $\bar{\zeta} = -\mathrm{Re}(s)/\mathrm{Im}(s) = \cot\theta$, in contrast to the damping ratio used in control theory, $\zeta = -\mathrm{Re}(s)/|s| = \cos\theta = \bar{\zeta}/\sqrt{1+\bar{\zeta}^2}$. The selection of the cotangent function to define the damping ratio simplifies the modifications required in the flutter analysis computer program described below. For small damping ratios the two definitions are asymptotic. For instance, with $\theta = 70°$, they differ by only 6 percent.

The integral in equation (3) exists for growing and for constant-amplitude motion, but for decaying motion the integral is improper. This problem is surmounted

as follows. For both growing and constant-amplitude motion, the integrals defining the kernel function are computable. These integrals are recognized as representations of analytic functions, namely, Bessel and Struve functions. These analytic functions can then be used to evaluate the quantity represented by the integrals for decaying motion even though the integrals are nonconvergent. This use of analytic continuation is described, for example, by Carrier, Krook, and Pearson (1966) and cited by Edwards (1977). The evaluation of the improper integral for decaying motion is described in the appendix.

For the present report the FAST (Flutter Analysis System) computer program of Desmarais and Bennett (1978) was modified to incorporate the generalized kernel function. The resulting aerodynamic forces are those corresponding to the user-selected $\bar{\zeta}$. The 12-term exponential series approximation D12.1 (see appendix) of Desmarais (1982) was used, in general. Several checks to verify accuracy were made with the 24-term series D24.2. As shown in the appendix, approximation D12.1 is accurate for growing and decaying motion in the s-plane extending at least 45° on both sides of the imaginary s-axis that represents harmonic motion.

Equations of Dynamic Equilibrium

In equation (22) of Cunningham (1978), the equations of equilibrium are given for growing and decaying motion. An equilibrium condition exists when the complex structural forces are balanced by the complex unsteady aerodynamic forces. Solutions can be obtained by an application of the familiar V-g root-finding technique. In this method aerodynamic forces are calculated for an assumed complex reduced frequency, and an eigenvalue problem is solved to determine the roots of the equilibrium equations. In general, none of the roots match the assumed reduced frequency and a matched condition must be determined by iteration. This procedure was implemented by modifying the solution procedure used for the traditional V-g root-finding technique in the FAST computer program of Desmarais and Bennett (1978).

Equation (5) of Desmarais and Bennett (1978) expresses the equilibrium condition at a flutter boundary, with motion neither growing nor decaying, for which solutions are obtained in the FAST program. This equation and program can be generalized to solve equation (22) of Cunningham (1978) for boundaries of selected $\bar{\zeta} \neq 0$, (as well as for $\bar{\zeta} = 0$). This generalization is done by replacing ω and k by $\omega(1 + i\bar{\zeta})$ and $k(1 + i\bar{\zeta})$ throughout the analysis. The resulting equations can be put in the form

$$\left[-\Omega + \left(\frac{\omega_o}{\omega_i}\right)^2 \frac{k^2(1 + i\bar{\zeta})^2}{(1 + ig_i)} \right] q_i + \frac{(\omega_o/\omega_i)^2}{m_i(1 + ig_i)} \frac{\rho \ell^4}{2} \sum_{j=1}^{N} \frac{q_j}{\ell} \bar{A}_{ij} = 0$$

$$(i = 1, 2, 3, \ldots, N) \qquad (4)$$

where the generalized aerodynamic force element

$$\bar{A}_{ij} \equiv \int_S \int h_i(x,y) \frac{\Delta p_j(x,y)}{\rho V^2/2} \, dx \, dy \qquad (5)$$

is a function of M, k, $\bar{\zeta}$, and the planform. The eigenvalues (one for each elastic mode)

$$\Omega \equiv \left(\frac{\omega_o \ell}{V}\right)^2 (1 + ig)$$

are sought at values of k for which the structural damping $g = 0$. Traditionally, solutions with $g \neq 0$, which are obtained in the iterative process of finding a matched flutter point, have been used as an indication of the approach to flutter. For the present study the only changes in the equilibrium equations (4) from those of Desmarais and Bennett (1978) are the factor of $(1 + i\bar{\zeta})^2$ in the second term and the $\bar{A}_{ij}$, which are now functions of $\bar{\zeta}$.

A Rational Function Approximation (RFA) of Unsteady Aerodynamic Forces

Sevart (1975), Roger (1977), and Abel (1979) described a mathematical technique used in control theory for approximating the unsteady aerodynamic forces in the general s-plane based on the forces for simple harmonic motion. The technique is outlined as follows:

1. Beginning with simple harmonic motion, each individual generalized-force matrix element $\bar{A}_{ij}$ of equations (4) is calculated for a series of values of ik

(note the distinction between the modal index i (in $\bar{A}_{ij}$) and the imaginary unit $i \equiv \sqrt{-1}$ (in ik)).

2. Using temporarily here the notation of Abel (1979), namely, $\hat{Q}(ik)$ to represent any individual $\bar{A}_{ij}(ik)$, the variation of the aerodynamic forces is approximated

by a rational function (RFA) with real coefficients of the form

$$\hat{Q}(ik) \approx A_0 + ikA_1 + (ik)^2 A_2 + \sum_{m=3}^{6} \frac{(ik)A_m}{ik + \beta_{m-2}} \tag{6}$$

3. Using known values of $\hat{Q}$ at a sequence of at least four values of k, a least-square-error solution for the real coefficients A_0 to A_6 is calculated. (The resulting approximations can be compared with the exact (input) values of k and also calculated for intermediate values of k.)

4. Substitute the complex quantity $s\ell/V$ for ik in equation (6) to obtain

$$\hat{Q}(s\ell/V) = A_0 + (s\ell/V)A_1 + (s\ell/V)^2 A_2 + \sum_{m=3}^{6} \frac{A_m s}{s + (V/\ell)\beta_{m-2}} \tag{7}$$

where

$$s \equiv \omega(-\bar{\zeta} + i) = i\omega(1 + i\bar{\zeta}) \tag{8}$$

and the damping ratio (positive for decaying motion) is

$$\bar{\zeta} \equiv \frac{\delta}{2\pi} = \cot \theta \tag{9}$$

In the present report all the results from the RFA were calculated using β_{m-2} as 0.2, 0.4, 0.6, and 0.8.

RESULTS AND DISCUSSION

Three flutter analyses were performed using the FAST program modified for growing and decaying motion as described above. The planforms analyzed, depicted in figure 1, are as follows: (1) a clipped-tip delta wing, (2) an aspect-ratio-five rectangular-planform model, and (3) a transport-type supercritical wing. Results of the present analysis, using the generalized kernel function, are compared with results of two approximate methods for calculating motion-damping ratios. One of these is the traditional V-g calculation of Smilg and Wasserman (1942). The other is the RFA aerodynamic-force method described in the preceding section. In all cases b_o was used for the reference length ℓ.

Clipped-Tip Delta-Wing Flutter Model

The clipped-tip delta-wing flutter model analyzed is that of the sample case of Desmarais and Bennett (1978), and the planform and aeroelastic parameters are given therein. The same model was analyzed at supersonic Mach numbers in Cunningham (1978). Figure 2 is a plot of speed index versus density for $M = 0.8$. Kernel-function results are shown at constant damping ratios $\bar{\zeta}$ for harmonic motion ($\bar{\zeta} = 0$), for growing motion ($\bar{\zeta} = -0.02$), and for decaying motion ($\bar{\zeta} = 0.02$ and 0.05), all with modal damping coefficients $g_i = 0$. For comparison the results of the V-g method are given by the dashed curves. In the V-g method the aerodynamic forces for $\bar{\zeta} = 0$ are used, and the value of g_i (the same for all modes i) corresponds to damping ratio $-2\bar{\zeta}$. The dashed curves were therefore computed with the coefficients $g_i = -0.04$ and -0.10 to forecast decaying motion and with $g_i = 0.04$ to forecast growing motion.

The figure includes a possible wind-tunnel operating curve for fixed Mach number M and speed of sound a_s. The intersections of the operating curve with the various boundaries are projected down to an inset plot of $\bar{\zeta}$ and $-g_i/2$ versus density. To avoid clutter, only five of eight projected points are indicated by the short-dashed lines. This plot reveals for this case that along the illustrated tunnel operating curve near the flutter condition, the gradient of damping ratio with respect to increasing density is only about half as steep for the correct aerodynamics ($\bar{\zeta}$ variable) as it is for simple harmonic aerodynamics ($\bar{\zeta} = 0$); thus the correct aerodynamics predict a less abrupt approach to flutter.

Figure 3 shows curves of the speed index for constant damping ratio versus Mach number for M ranging from 0.5 to 0.9. The values of speed index from figure 2 for $\rho = 0.002378$ slug/ft^3 are included. At $M = 0.5$, there is very little difference between the solid-curve and the dashed-curve predictions of speed index for the two damping ratios analyzed, which are above and below the flutter boundary. As M increases toward 0.9, the two predictions become more different, with the present

variable-$\bar{\zeta}$ aerodynamics predicting a lower rate of change of damping ratio versus speed index at a given Mach number than does the V-g analysis with $\bar{\zeta} = 0$ and variable g_i.

Aspect-Ratio-Five Rectangular-Planform Model

Aerodynamic-force results.- Doggett, Rainey, and Morgan (1959) tested this model at several Mach numbers. Yates et al. (1982) reported recent flutter analyses via two subsonic aerodynamic programs and compared the analytical and experimental results in figures 14 to 16 therein. One of the programs used was the unmodified FAST program of Desmarais and Bennett (1978). Three bending and two torsion modes of a uniform cantilever beam were utilized.

With the present modified FAST program, aerodynamic forces were calculated for three decay ratios, namely, $\bar{\zeta} = 0$ and ± 0.1, and for a range of reduced frequencies k from 0 to 0.228. (The flutter experiments had values of k ranging from 0.047 to 0.102.) For one of the experimental Mach numbers, $M = 0.904$, two of the generalized forces $\bar{A}_{12}$ and $\bar{A}_{22}$ are plotted in figure 4. The kernel-function results are indicated by "K" in the figure. Figure 4(a) shows $\bar{A}_{22}$, descriptively termed the "weighted twisting moment due to first-torsion-mode vibration." The curve for harmonic motion, $\bar{\zeta} = 0$, reflects the effects induced by the past history of constant-amplitude motion, and the moment lags in phase behind the torsional deflection. The negative imaginary part indicates that this moment of itself acts to damp out the first torsion component of motion. The positive real part indicates that the moment $\bar{A}_{22}$ acts to increase, or diverge, the torsional displacement, and thus to decrease the first torsional frequency as the dynamic pressure increases. The curve for $\bar{\zeta} = 0.1$ reflects the effects induced by a past history of exponentially decaying motion, while the curve for $\bar{\zeta} = -0.1$ reflects the effects induced by a past history of growing motion. The three vectors from the origin to the points for $k = 0.114$ show that the moment $\bar{A}_{22}$ lags the torsional displacement a little more for decaying motion and a little less for growing motion than it does for constant-amplitude motion. Thus to the extent that the wing torsional motion component influences the overall flutter motion, the variation of the lag of the moment $\bar{A}_{22}$ with $\bar{\zeta}$ contributes in the same sense as $\bar{\zeta}$; that is, decaying motion is accompanied by an increased decay-producing moment, and growing motion by a decreased decay-producing moment. For comparison the plus (+) symbols were computed from equation (7). The seven coefficients of the RFA of equation (7) were computed by substituting the $\bar{A}_{22}$ for the five values of k with $\bar{\zeta} = 0$ into equation (6). The RFA results compare favorably with kernel-function results in this application.

Figure 4(b) shows $\bar{A}_{12}$, the weighted lift due to first-torsion-mode motion (note that the horizontal scale begins at 24). As with the moment $\bar{A}_{22}$, this lift quantity displays more phase lag with decaying motion, and less phase lag and even a phase lead with growing motion in comparison to constant-amplitude motion. As in figure 4(a) the comparison between kernel-function and RFA results is good.

Flutter and damping-ratio boundaries.- Next the flutter boundary and selected damping-ratio boundaries for growing and decaying motion near the flutter boundary were calculated for this four-percent-thick rectangular model. This was done for four of the Mach numbers, namely, $M = 0.756$, 0.801, 0.856, and 0.904, listed in table III of Doggett, Rainey, and Morgan (1959). The model properties from their table 1(a) for the first and second bending and first torsion modes were used; however, because the modal damping coefficients g_i for first and second bending modes of the four-percent-thick wing are missing, those coefficients for the six-percent-thick wing were used from table 1(a). Calculated mode shapes for a uniform cantilever beam with midchord center of gravity and elastic axis were used. Moreover, the next two high frequency calculated modes, namely, second torsion and third bending, were included to ensure convergence of results with respect to the number of modes. For each of the four Mach numbers the density at the experimental flutter point was used.

Figure 5 shows flutter boundary ($\bar{\zeta} = 0$) as the flutter speed index $(V/b_o\omega_\alpha\sqrt{\mu})$ plotted against Mach number. The higher and lower boundaries are for $\bar{\zeta} = -0.025$ and 0.025, respectively. The comparison points from the RFA of equation (7) are very close to those from the kernel function.

Two-Dimensional Wing Section

Early studies of the DAST high-aspect-ratio transport wing model (see the following section) produced unexpected wavy and looping curves of the complex generalized forces as functions of reduced frequency for decaying motion. This behavior cast doubt on the adequacy of the computational process, including the convergence with respect to the downwash collocation order. Since collocation order can be extended very high for two-dimensional flow, aerodynamic forces were studied for the oscillating two-dimensional wing section to determine whether similar trends would be calculated and to test for convergence with respect to the number of downwash collocation points. Edwards (1979) presents similar examples of section lift due to plunging and pressure distributions resulting from both growing and decaying airfoil motions.

For the present report the classical Possio integral equation formulation as described in Bland (1982) was used. The associated computer program for harmonic motion was generalized to growing and decaying exponential motion. For most of the two-dimensional section calculations, 64 downwash collocation points were used. Figure 6 shows the section lift due to plunging and pitching oscillations for $M = 0.9$ and for three motion-decay ratios, namely, (1) simple harmonic motion ($\bar{\zeta} = 0$), (2) growing motion with $\bar{\zeta} = -0.1$, and (3) decaying motion with $\bar{\zeta} = 0.1$. Results from both the generalized kernel-function calculation (denoted "K") and the RFA (based on 14 values of k) are included. The range of reduced frequency is large, from 0 to 4.0.

Figure 6(a) shows $\bar{A}_{11}$, the generalized lift due to plunging. (The plunge half-amplitude is the semichord length.) The kernel-function results for $\bar{\zeta} = 0$ agree rather well with the RFA results of equation (7). The RFA results for growing motion, $\bar{\zeta} = -0.1$, also agree well with the kernel-function results.

For decaying motion, $\bar{\zeta} = 0.1$, the RFA of equation (7) is given by the smooth dashed curve. In great contrast is the looping curve of the kernel-function result. Certain values of k are labeled. As k increases beyond about 0.9, the curve

first develops a wavy behavior, then a near cusp, and finally widening loops. This unexpected wavy and looping behavior appears for values of k that are well beyond almost any wing flutter, but which might be reached for control-surface flutter.

Figures 6(b) and 6(c) show the generalized lift $\bar{A}_{12}$ due to pitching about the quarter-chord with half-amplitude of 1 radian. Figure 6(b) shows the kernel-function result for $\bar{\zeta} = 0$ and -0.1 from $k = 0$ to 5.0 and for $\bar{\zeta} = 0.1$ from $k = 0$ to 0.5. It is apparent that the seven-term RFA function of equation (7) fitted to the 14 values of this particular $\bar{A}_{12}$ does not result in a good fit. This inadequate fit is due to the reversal of $\bar{A}_{12}$ in the selected range of k and to the least-square-error fit being over too great a range of k. An improvement would be needed for RFA applications. The spread for the three values of $\bar{\zeta}$ is as expected except for the looping near $k = 0.5$. Figure 6(c) gives an enlarged view of the behavior of $\bar{A}_{12}$ for the frequency range $0.5 \leq k \leq 4.5$. The wavy behavior for $\bar{\zeta} = 0.1$ begins near $k = 0.5$ and becomes looping behavior for k greater than about 1.0.

As stated above, all the results shown were calculated with 64 collocation points on the chord. Checks were also made with 32 and 128 collocation points, and only insignificant differences were found even to $k = 4.0$. The conclusion is reached therefore that the kernel-function results shown are converged with respect to the number of collocation points, and that the looping behavior calculated for decaying motion with $\bar{\zeta} = 0.1$ is a valid mathematical result. This looping behavior occurs for values of k well above the range of most wing flutter, except possibly control-surface flutter. It may be applicable to gust analysis that extends to high values of k.

The DAST ARW-1 High-Aspect-Ratio Swept Wing

The most realistic model analyzed here is the DAST ARW-1 (from Drones for Aerodynamic and Structural Testing, aeroelastic research wing 1); see Murrow and Eckstrom (1979). The planform analyzed is shown in figure 1. It is essentially the planform shown in figure 2 of Newsom and Pototzky (1982), but no aerodynamic effects of horizontal or vertical tail surfaces or of a fuselage are included. The 12 spanwise symmetric mode shapes and frequencies employed are those calculated for the original DAST ARW-1 wing via the NASTRAN[2] finite-element analysis that was reported in Newsom and Pototzky (1982). These modes consist of 2 rigid-body (vertical translation and pitch) and the first 10 elastic modes, not including any aileron motion. The aileron hinge is treated as locked (no aileron rotation).

Aerodynamic-force results.- Figure 7 shows the $\bar{A}_{55}$ from kernel-function results and the RFA (based on nine values of k) for the damping ratios $\bar{\zeta} = 0, \pm 0.1$, and ± 0.577 $(\tan(\pm 30°))$ for $0 \leq k \leq 1.0$ and $M = 0.8$. Mode 5 (the third elastic mode), although strongly coupled, is judged to be best described as "first torsion." The original ARW-1 wing described by Edwards (1979) and Newsom and Pototzky (1982) experienced flutter during flight testing at $k \approx 0.16$.

---

[2]NASTRAN is a registered trademark of the National Aeronautics and Space Administration.

The looping behavior of the kernel-function result for $\bar{\zeta} = 0.577$ is like the looping of the two-dimensional case described in a preceding section and is believed to be a valid result. The RFA result agrees with the kernel-function result except for the highly damped motion ($\bar{\zeta} = 0.577$) at values of k about 0.2 and higher, especially for k higher than 0.3.

Flutter analysis results.- The present flutter analysis employs the subsonic kernel-function aerodynamics generalized to growing and decaying motion. Newsom and Pototzky (1982) reported the flutter and preflutter results obtained based on doublet-lattice aerodynamics for simple harmonic motion and extrapolation into the complex s-plane via the RFA.

The technique of strengthening the analytical aerodynamic forces by multiplying by the ratio of wind-tunnel static lift to the analytical static lift employed by Newsom and Pototzky (1982) is used in the present analysis. The upper curve of C_{L_α} versus M in figure 8 herein is from figure 17 of Byrdsong and Hallissy (1979) and is for the complete model including the horizontal tail. Since the analysis here is of the wing only, the second curve of figure 8 was obtained from the tail-off data (plots of C_L vs. α) of figures 11(a) to 11(e) of Byrdsong and Hallissy (1979). The lowest curve of figure 8 is from the kernel-function program using program-default downwash collocation at 6 chord stations on each of 12 span stations. The difference in percent from the bottom (analytical) curve up to the tail-off experimental curve is indicated for several Mach numbers; this difference was used to strengthen the generalized force matrix in the flutter analysis.

Flutter stability was analyzed at Mach numbers from 0.70 up to 0.82 for 15000 feet and up to 0.94 for 25000 feet. Densities and sound speeds were used from the U.S. Standard Atmosphere, 1962. Figure 9(a) for 15000 feet and figure 9(b) for 25000 feet show the calculated damping ratio $\bar{\zeta}$ and associated frequency f versus Mach number. The circles are the experimental values that appear in figures 8 and 10 of Newsom and Pototzky (1982), and the flight flutter point from their figure 10 is shown by the arrow. The good correlation of the present analysis and experiment is evident. The analytical results of Newsom and Pototzky (1982), based on doublet-lattice aerodynamics with the strengthening of their figure 5, are given by the dashed curves. As can be observed, these results are comparable to those of the present analysis and to the flight experiments.

CONCLUDING REMARKS

The subsonic kernel function has been generalized to the s-plane for growing and decaying oscillatory motion. The function was substituted into a flutter analysis program, and that program was also adapted throughout to obtain the desired solutions for constant-damping-ratio boundaries, including the usual zero-decay flutter boundary. A rational function approximation (RFA) used in control theory for approximating s-plane aerodynamic forces was used for some comparisons.

For the cases analyzed, the RFA aerodynamics gave (or could give) very good agreement with the s-plane subsonic-kernel-function results for the lower reduced frequencies that characterize wing flutter. But for combinations of higher damping ratios and of higher frequencies that often characterize control-surface flutter, the RFA aerodynamics did not follow the looping and spiraling kernel-function results.

For a clipped-tip delta-wing flutter model, the s-plane kernel function predicted a less steep gradient of damping ratio versus density as the flutter boundary was approached and exceeded than did the conventional V-g solution method that uses simple harmonic aerodynamics.

An aspect-ratio-five rectangular-planform model was analyzed for four Mach numbers (M) ranging from 0.756 to 0.904. Constant-damping-ratio boundaries, one for decaying and one for growing motion, are presented near the flutter boundary. At M = 0.904, study of the weighted torsional moment due to first-torsion-mode oscillation showed that in comparison to the phase lagging moment of constant-amplitude motion, decay produced a greater lag of that moment, while growth produced a lesser lag. Thus, in terms of this first torsion moment only, decay promotes faster decay, and growth promotes slower decay; but for coupled-mode flutter there is no assurance that the overall flutter motion will show this same effect. The RFA aerodynamics gave good comparisons for both aerodynamic forces and decay-ratio results for the low reduced frequencies studied.

An analysis of the DAST ARW-1[3] transport-type wing was also made. Plots of damping ratio versus flight Mach number were calculated for two altitudes, 15000 and 25000 feet. Good comparisons of damping ratios and associated frequencies were obtained with flight experiments and also with a doublet-lattice analysis that used the RFA. The same type of analytical treatment was used here as was used in a referenced doublet-lattice analysis; namely, in the flutter analysis the generalized forces were strengthened by multiplying by the ratio of the lift-curve slope C_{L_α} obtained on a wind-tunnel model (tail off) to that from the subsonic-kernel-function aerodynamics. For M = 0.8 and reduced frequencies ranging from 0 to 1.0 the generalized "first-torsion-mode" forces calculated from the kernel function agreed with those calculated from the rational function approximation (as in Abel, NASA TP-1367, 1979, for example) except at large damping ratios.

At reduced frequencies higher than that of the experimental flutter, an unexpected doubling back and looping of some of the generalized forces for strongly decaying motion were found in the complex plane. This behavior cast doubt on the adequacy of the computational process for the DAST wing, including the convergence with respect to the downwash collocation order. Therefore the two-dimensional-flow wing section was studied because the collocation order can be extended very high and collocation convergence can be studied. The classical Possio integral equation formulation was used. An existing computer program for harmonic motion was generalized to growing and decaying motion. For moderately decaying motion a looping behavior of the lift forces due to both translational and pitching oscillations was found at higher reduced frequencies for collocation-converged results. Because of these two-dimensional-flow results the similar behavior for the DAST ARW-1 in three-dimensional flow at high reduced frequencies and high damping ratio is concluded to be valid. In any event the reduced frequency of flutter is well below that of the looping behavior. The RFA aerodynamics did not follow the looping behavior at higher reduced frequencies.

In the appendix, procedures were described and evaluated for the accurate calculation of the kernel function for general s-plane motion. A 12-term exponential

---

[3]Drones for Aerodynamic and Structural Testing (DAST), aeroelastic research wing 1 (ARW-1).

series approximation in the kernel-function integral was shown to provide good accuracy for growing and decaying motion in the s-plane extending at least 45° on both sides of the imaginary s-axis that represents harmonic motion.

Langley Research Center
National Aeronautics and Space Administration
Hampton, VA 23665
February 17, 1984

APPENDIX

CALCULATION OF THE SUBSONIC KERNEL FUNCTION IN THE s-PLANE

This appendix serves four purposes. It describes the algorithm used in this report to compute the kernel of the downwash integral equation. It indicates in what part of the complex s-plane the algorithm gives acceptable results. It explains why this particular algorithm was used. It also explains why the algorithm used, or any similar algorithm, cannot be expected to give good results for all complex values of reduced frequency.

The kernel function, essentially as in equation (3) but with k replaced by k_c, is

$$K(M,k_c,x_o,y_o) = \frac{\bar{K}(M,k_c,x_o,y_o)}{\ell^2 y_o^2}$$

where

$$\bar{K}(M,k_c,x_o,y_o) = \exp(-ik_c x_o)\left[\left(1 + \frac{x_o}{R}\right)\exp\left(-ik_c u_1 |y_o|\right) - ik_c|y_o| \int_{u_1}^{\infty} \left(1 - \frac{u}{\sqrt{1+u^2}}\right)\exp\left(-ik_c|y_o|u\right) du\right] \tag{A1}$$

and where k_c is the complex reduced frequency

$$k_c = k(1 + i\bar{\zeta})$$

and

$$R = \sqrt{x_o^2 + \beta^2 y_o^2}$$

$$u_1 = (-x_o + MR)\Big/(\beta^2|y_o|)$$

In equation (A1) let

$$\bar{s} = ik_c = s\ell/V \tag{A2}$$

Then

$$\bar{K}(M,-i\bar{s},x_o,y_o) = \exp(-\bar{s}x_o)\left[\left(1 + \frac{x_o}{R}\right)\exp(-\bar{s}u_1|y_o|) - F(\bar{s}|y_o|)\right] \tag{A3}$$

where

$$F(z) = z\int_{u_1}^{\infty}\left(1 - \frac{u}{\sqrt{1+u^2}}\right)\exp(-zu)\,du \tag{A4}$$

and the symbol $z \equiv s|y_o|$ is not the z of the main text. Integral equation (A4) defines the function $F(z)$ only for $|\arg z| < \pi/2$. For the multileaved Riemann surface, $|\arg z| > \pi/2$, $F(z)$ is defined by analytic continuation as follows:

$$F(z) = F_1(z) - F_2(z)$$

where

$$F_1(z) = z\int_0^{\infty}\left(1 - \frac{u}{\sqrt{1+u^2}}\right)\exp(-zu)\,du$$

$$F_2(z) = z\int_0^{u_1}\left(1 - \frac{u}{\sqrt{1+u^2}}\right)\exp(-zu)\,du$$

By integrating by parts and applying equations 12.1.8, 12.1.9, and 9.1.5 of Abramowitz and Stegun (1964), one obtains

$$F_1(z) = 1 + z - \frac{\pi}{2}z\,H_1(z) + \frac{\pi}{2}z\,Y_1(z) \tag{A5}$$

where $H_1(z)$ is a Struve function and $Y_1(z)$ is a Bessel function of the second kind. To show the analytic behavior of $F_2(z)$, expand $\exp(-zu)$ into a power series and integrate termwise to obtain

$$F_2(z) = \sum_{m=0}^{\infty}\frac{(-1)^m g_m}{m!}z^{m+1} \tag{A6}$$

where

$$g_m = \int_0^{u_1} \left(1 - \frac{u}{\sqrt{1 + u^2}}\right) u^m \, du$$

Since $|g_m|$ is bounded by $|u_1|^{m+1}/(m + 1)$, the series (eq. (A6)) has an infinite radius of convergence, and hence $F_2(z)$ is an entire analytic function. In equation (A5), the Struve function $z\,H_1(z)$ is also an entire analytic function. The Bessel function $z\,Y_1(z)$ can be expressed

$$z\,Y_1(z) = \frac{2}{\pi} z\,J_1(z)\,\ln\frac{z}{2} + G(z)$$

where $z\,J_1(z)$ and $G(z)$ are both entire analytic functions of z. Thus equations (A5) and (A6) furnish an analytic continuation of $F(z)$ into the multileaved Riemann surface $|\arg z| > \pi/2$.

There are no singularities in $F(z)$ in the finite part of the complex plane except for a logarithmic branch point at $z = 0$. The natural branch cut of $F(z)$ is the natural branch cut of $\ln z/2$, namely, the negative real z-axis.

The integral of equation (A4) is evaluated numerically by replacing the algebraic part of the integrand by an exponential approximation and integrating termwise:

$$1 - \frac{u}{\sqrt{1 + u^2}} \approx \sum_{\ell=1}^{12} a_\ell \exp(-2^\ell bu) \qquad (0 \leq u < \infty) \qquad \text{(A7)}$$

An approximation of this sort is used for several reasons: (1) it is a function of a single variable; (2) only one exponential is needed per kernel function, contributing to economy of calculation; (3) a modest number of terms provide nearly single-precision computer-word accuracy for harmonic motion; and (4) as described below, good accuracy extends to rather large damping ratios. The coefficients in equation (A7), namely,

$$b = 0.009054814793$$

$a_1 = 0.000319759140$	$a_2 = -0.000055461471$
$a_3 = 0.002726074362$	$a_4 = 0.005749551566$
$a_5 = 0.031455895072$	$a_6 = 0.106031126212$
$a_7 = 0.406838011567$	$a_8 = 0.798112357155$
$a_9 = -0.417749229098$	$a_{10} = 0.077480713894$
$a_{11} = -0.012677284771$	$a_{12} = 0.001787032960$

are for the approximation (eq. (A7)) designated D12.1 by Desmarais (1982). Then, if $u_1 \geq 0$,

$$F(\bar{s}|y_o|) \approx \bar{s}|y_o| \exp(-\bar{s}u_1|y_o|) \sum_{\ell=1}^{12} \frac{a_\ell e_\ell}{2^\ell b + \bar{s}|y_o|} \tag{A8}$$

where

$$e_1 \equiv \exp(-bu_1)$$

$$e_\ell \equiv (e_{\ell-1})^2 \qquad (\ell = 2 \text{ to } 12)$$

The closed-form integrals that were used to derive equation (A8) all converge only if $\mathrm{Re}(\bar{s}|y_o|) > -b$. For lower values of $\mathrm{Re}(\bar{s}|y_o|)$, equation (A8) is deduced by analytic continuation.

Since approximation D12.1 is valid only for $u \geq 0$, another approximation to $F(\bar{s}|y_o|)$ is used for $u_1 < 0$:

$$F(\bar{s}|y_o|) \approx -2 - 2(\bar{s}y_o)^2 \sum_{\ell=1}^{12} \frac{a_\ell}{(2^\ell b)^2 - (\bar{s}y_o)^2} + \exp(-\bar{s}u_1|y_o|) \left(2 + \sum_{\ell=1}^{12} \frac{a_\ell \bar{e}_\ell}{2^\ell b - \bar{s}|y_o|} \right) \tag{A9}$$

where

$$\bar{e}_1 \equiv \exp(bu_1)$$

$$\bar{e}_\ell \equiv (\bar{e}_{\ell-1})^2 \qquad (\ell = 2 \text{ to } 12)$$

Approximation (A8) has poles at

$$\bar{s}|y_o| = -2^\ell b \qquad (\ell = 1 \text{ to } 12)$$

that is, on the negative real $\bar{s}$-axis, and approximation (A9) has poles at

$$\bar{s}|y_o| = \pm 2^\ell b \qquad (\ell = 1 \text{ to } 12)$$

that is, on the negative and positive real $\bar{s}$-axes. The function $F(\bar{s}|y_o|)$ has no singularities except a branch point at $\bar{s}|y_o| = 0$. Thus one would expect approximation (A8) to become unusable as $\arg \bar{s}$ approaches $\pm\pi$, and approximation (A9) to behave similarly as $\arg \bar{s}$ approaches either $\pm\pi$ or 0. This is shown in figure 10(a). These are plots of the real and imaginary parts of $\bar{K}$ versus $|k_c y_o|$ for $|k_c y_o| = 0$ to 8 and $u_1 = 0$. The exact $\bar{K}$ (solid line) is compared with the approximation (dashed line). The value of u_1 is zero so that the exact $\bar{K}$ is easily computed from equation (A5). For $\theta = \pi/8$, the exact and approximate curves are almost indistinguishable. For $\theta = \pi/4$, the error is noticeable but approximation (A7) gives acceptable engineering accuracy. Figure 10(b) shows the same information for an earlier and commonly used exponential approximation similar to D12.1 presented in Laschka (1970) and designated L11 in Desmarais (1982). Approximation L11 is about as bad at $\theta = \pi/8$ as approximation D12.1 is at $\theta = \pi/4$. At $\theta = \pi/4$, approximation L11 is unacceptable. The lower plot of figure 10(b) also appears as part of figure 1 of Ashley and Boyd (1980) along with a still earlier approximation from Watkins, Woolston, and Cunningham (1959) designated W4 in Desmarais (1982). In Ashley and Boyd (1980), the poor performance of L11 and W4 for $\theta = \pi/4$ is attributed to the proximity of the poles of the computed kernel. However, approximation D12.1, which has poles along the same line as L11, performs very well at $\theta = \pi/4$. This is so because the error induced near a pole is proportional to the magnitude of the residue at that pole, and each residue is proportional to the associated coefficient a_ℓ. For approximation L11, $\max|a_\ell| = 644.8$, whereas for approximation D12.1, $\max|a_\ell| = 0.798$.

To sum up, if $|\theta| < \pi/4$, then equations (A8) and (A9), which use approximation D12.1, give acceptable accuracy. All calculations in this report used values of k_c for which $|\theta|$ was much less than $\pi/4$ and were performed using approximation D12.1 except for a few check calculations that were performed using approximation D24.2 of Desmarais (1982); and no significant differences were found. Approximation D24.2 is more accurate than D12.1 and takes about twice as long to execute.

It is the authors' opinion that exponential approximations, such as D12.1, for which $\max|a_k| < 1$, provide a satisfactory way of computing $\bar{K}(M,k_c,x_o,y_o)$ (where $k_c = -i\bar{s}$), to the accuracy needed for aerodynamic-force calculations, in the half of the complex s-plane for which either $|-\theta| < \pi/4$ or $|\theta| < \pi/4$; that is, for $\pi/4 < \arg \bar{s} < 3\pi/4$ and $-3\pi/4 < \arg \bar{s} < -\pi/4$. For the remainder of the complex s-plane, $|\arg \bar{s}| < \pi/4$ or $|\arg \bar{s}| > 3\pi/4$, estimates of $\bar{K}$ based on exponential approximations to $1 - (u/\sqrt{1 + u^2})$ become inaccurate or uneconomical, or both.

REFERENCES

Abel, Irving 1979: An Analytical Technique for Predicting the Characteristics of a Flexible Wing Equipped With an Active Flutter-Suppression System and Comparison With Wind-Tunnel Data. NASA TP-1367.

Abramowitz, Milton; and Stegun, Irene A., eds. 1964: Handbook of Mathematical Functions With Formulas, Graphs, and Mathematical Tables. NBS Appl. Math. Ser. 55, U.S. Dep. Commer., June. Also, Dover Publ. Inc., 1965.

Ashley, H.; and Boyd, W. W. 1980: On Choosing the Best Approximations for Unsteady Potential Theory. Proceedings of the Colloquium honoring Hans Georg Küssner, Institut für Aeroelastik, DFVLR (Göttingen, West Germany), Sept., pp. 25-44.

Bland, Samuel R. 1982: Development of Low-Frequency Kernel-Function Aerodynamics for Comparison With Time-Dependent Finite-Difference Methods. NASA TM-83283.

Byrdsong, Thomas A.; and Hallissy, James B. 1979: Longitudinal and Lateral Static Stability and Control Characteristics of a 1/6-Scale Model of a Remotely Piloted Research Vehicle With a Supercritical Wing. NASA TP-1360.

Carrier, George F.; Krook, Max; and Pearson, Carl E. 1966: Functions of a Complex Variable. McGraw-Hill, Inc.

Cunningham, Herbert J. 1978: Analysis of Preflutter and Postflutter Characteristics With Motion-Matched Aerodynamic Forces. NASA TP-1232.

Desmarais, Robert N. 1982: An Accurate and Efficient Method for Evaluating the Kernel of the Integral Equation Relating Pressure to Normalwash in Unsteady Potential Flow. A Collection of Technical Papers. Part 2: Structural Dynamics and Design Engineering - AIAA/ASME/ASCE/AHS 23rd Structures, Structural Dynamics and Materials Conference, May, pp. 243-255. (Available as AIAA-82-0687.)

Desmarais, Robert N.; and Bennett, Robert M. 1978: User's Guide for a Modular Flutter Analysis Software System (FAST Version 1.0). NASA TM-78720.

Doggett, Robert V., Jr.; Rainey, A. Gerald; and Morgan, Homer G. 1959: An Experimental Investigation of Aerodynamic Effects of Airfoil Thickness on Transonic Flutter Characteristics. NASA TM X-79.

Edwards, John W. 1979: Applications of Laplace Transform Methods to Airfoil Motion and Stability Calculations. Technical Papers on Structures and Materials - AIAA 20th Structures, Structural Dynamics, and Materials Conference, Apr., pp. 465-481. (Available as AIAA Paper 79-0772.)

Edwards, John William 1977: Unsteady Aerodynamic Modeling and Active Aeroelastic Control. SUDAAR 504 (Grant NGL-05-020-007), Guidance & Control Lab., Stanford Univ., Feb. (Available as NASA CR-148019.)

Küssner, H. G. 1940: Allgemeine Tragflächentheorie. Luftfahrtforschung, Bd. 17, Lfg. 11/12, Dec., pp. 370-378. Translation, NACA TM 979, 1941. Reprint, AIAA Selected Reprint Series - Volume V, Aerodynamic Flutter, I. E. Garrick, ed., AIAA, Mar. 1969, pp. 36-39.

Laschka, B. 1970: Interfering Lifting Surface in Subsonic Flow. Z. Flugwiss., vol. 18, Oct., pp. 359-368.

Murrow, H. N.; and Eckstrom, C. V. 1979: Drones for Aerodynamic and Structural Testing (DAST) - A Status Report. J. Aircr., vol. 16, no. 8, Aug., pp. 521-526.

Newsom, Jerry R.; and Pototzky, Anthony S. 1982: Analysis and Flight Data for a Drone Aircraft With Active Flutter Suppression. J. Aircr., vol. 19, no. 11, Nov., pp. 1012-1018.

Roger, Kenneth L. 1977: Airplane Math Modeling Methods for Active Control Design. Structural Aspects of Active Controls, AGARD-CP-228, Aug., pp. 4-1 - 4-11.

Sevart, Francis D. 1975: Development of Active Flutter Suppression Wind Tunnel Testing Technology. AFFDL-TR-74-126, U.S. Air Force, Jan. (Available from DTIC as AD B002 840L.)

Smilg, Benjamin; and Wasserman, Lee S. 1942: Application of Three-Dimensional Flutter Theory to Aircraft Structures. ACTR No. 4798, Materiel Div., Army Air Corps, July.

U.S. Standard Atmosphere, 1962. NASA, U.S. Air Force, and U.S. Weather Bur., Dec.

Watkins, Charles E.; Runyan, Harry L.; and Woolston, Donald S. 1955: On the Kernel Function of the Integral Equation Relating the Lift and Downwash Distributions of Oscillating Finite Wings in Subsonic Flow. NACA Rep. 1234. (Supersedes NACA TN 3131.)

Watkins, Charles E.; Woolston, Donald S.; and Cunningham, Herbert J. 1959: A Systematic Kernel Function Procedure for Determining Aerodynamic Forces on Oscillating or Steady Finite Wings at Subsonic Speeds. NASA TR R-48.

Yates, E. Carson, Jr.; Cunningham, Herbert J.; Desmarais, Robert N.; Silva, Walter A.; and Drobenko, Bohdan 1982: Subsonic Aerodynamic and Flutter Characteristics of Several Wings Calculated by the SOUSSA P1.1 Panel Method. AIAA-82-0727, May.

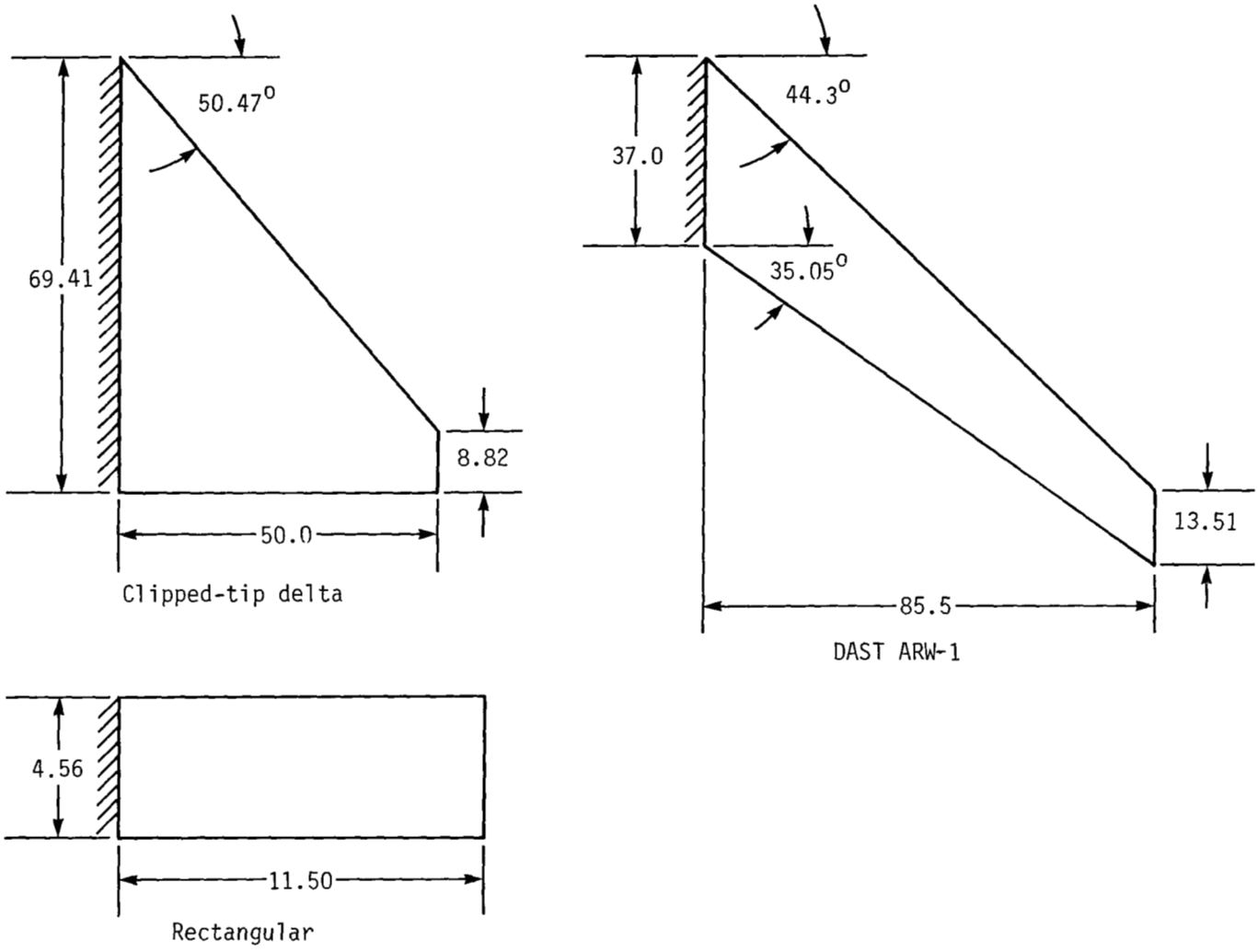

Figure 1.- Three planforms analyzed. Linear dimensions are in inches.

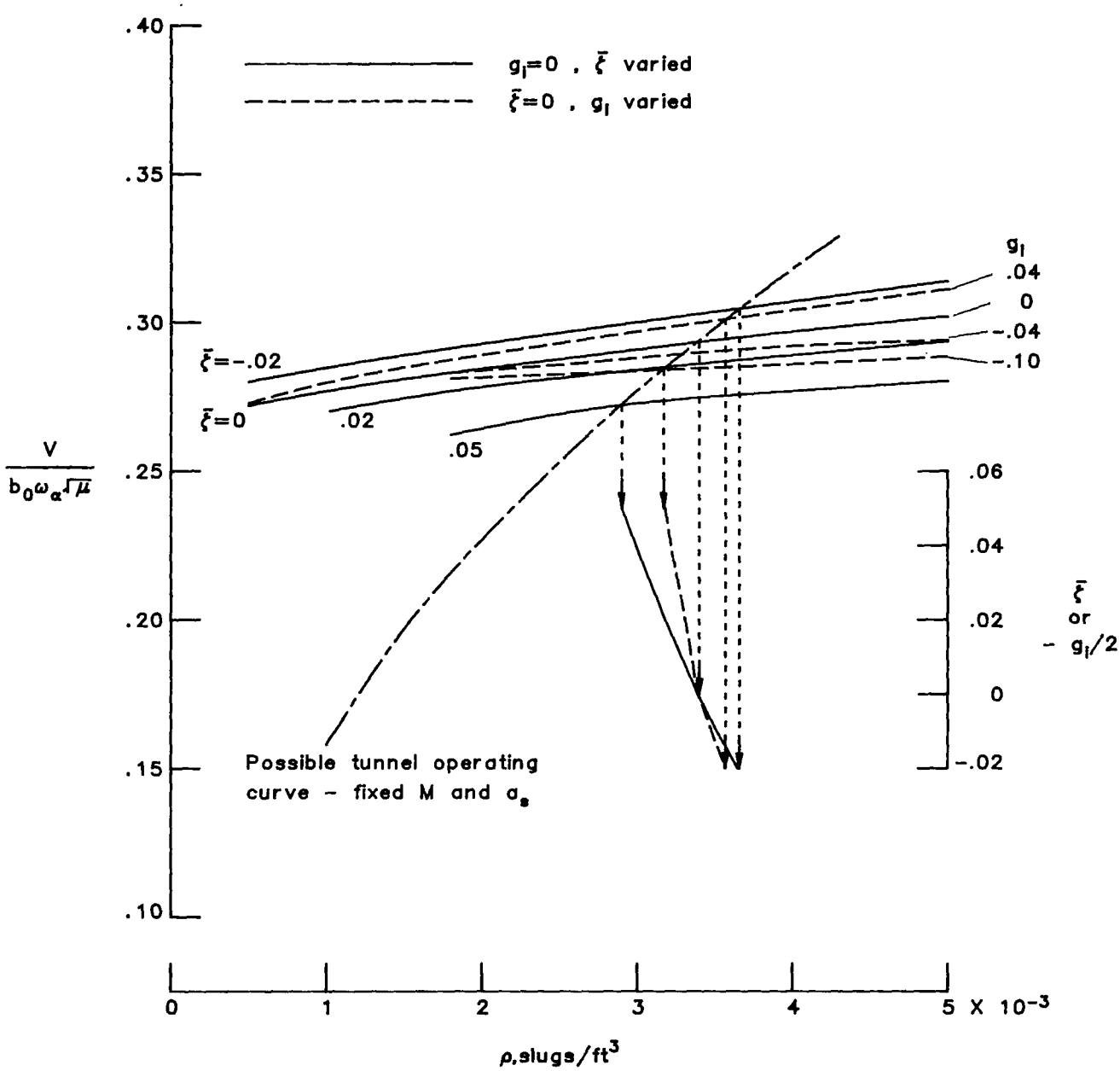

Figure 2.- Speed index versus density for clipped-tip delta-wing model. M = 0.8.

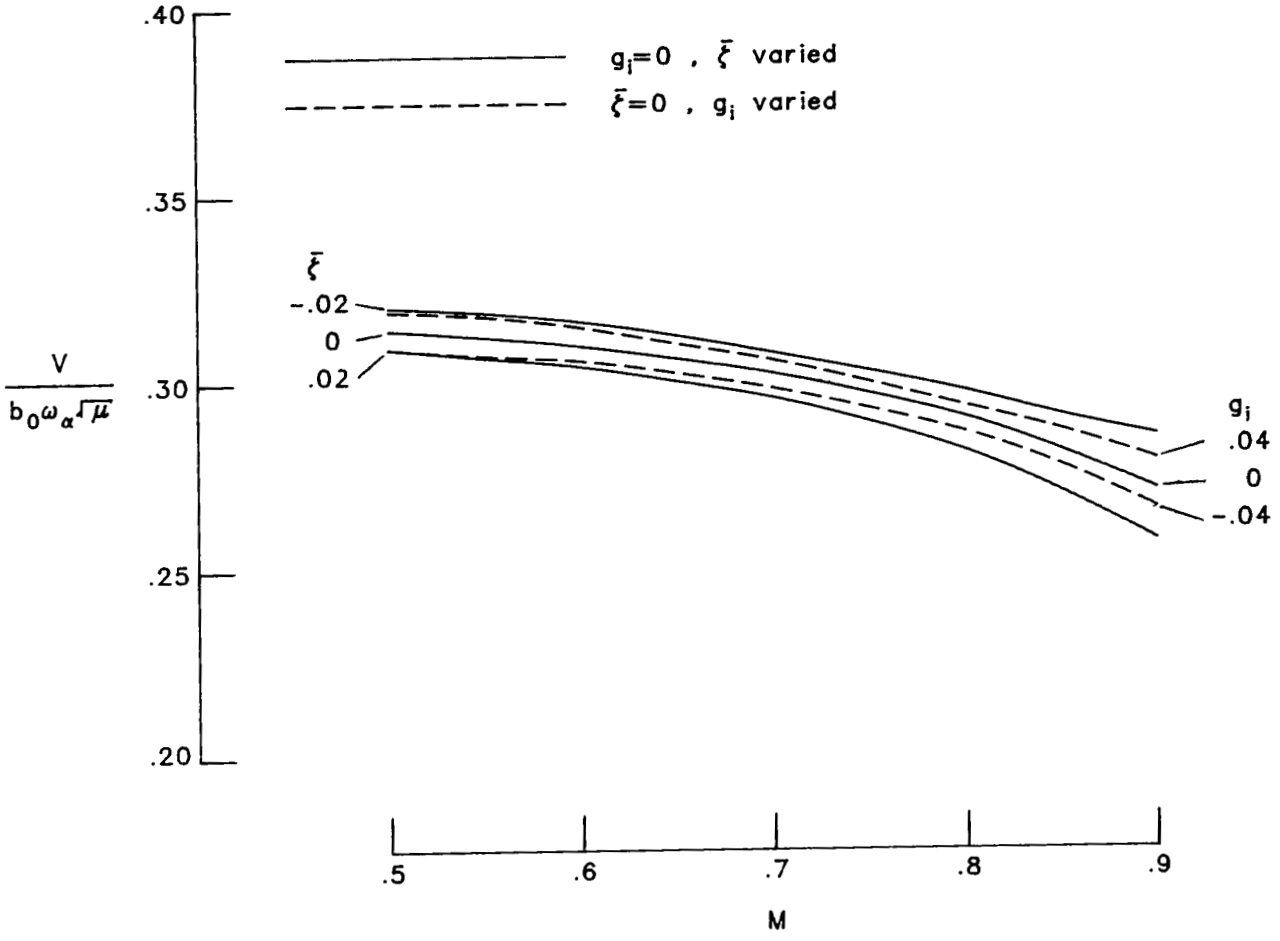

Figure 3.- Speed index versus Mach number for clipped-tip delta-wing model. ρ = 0.002378 slug/ft^3.

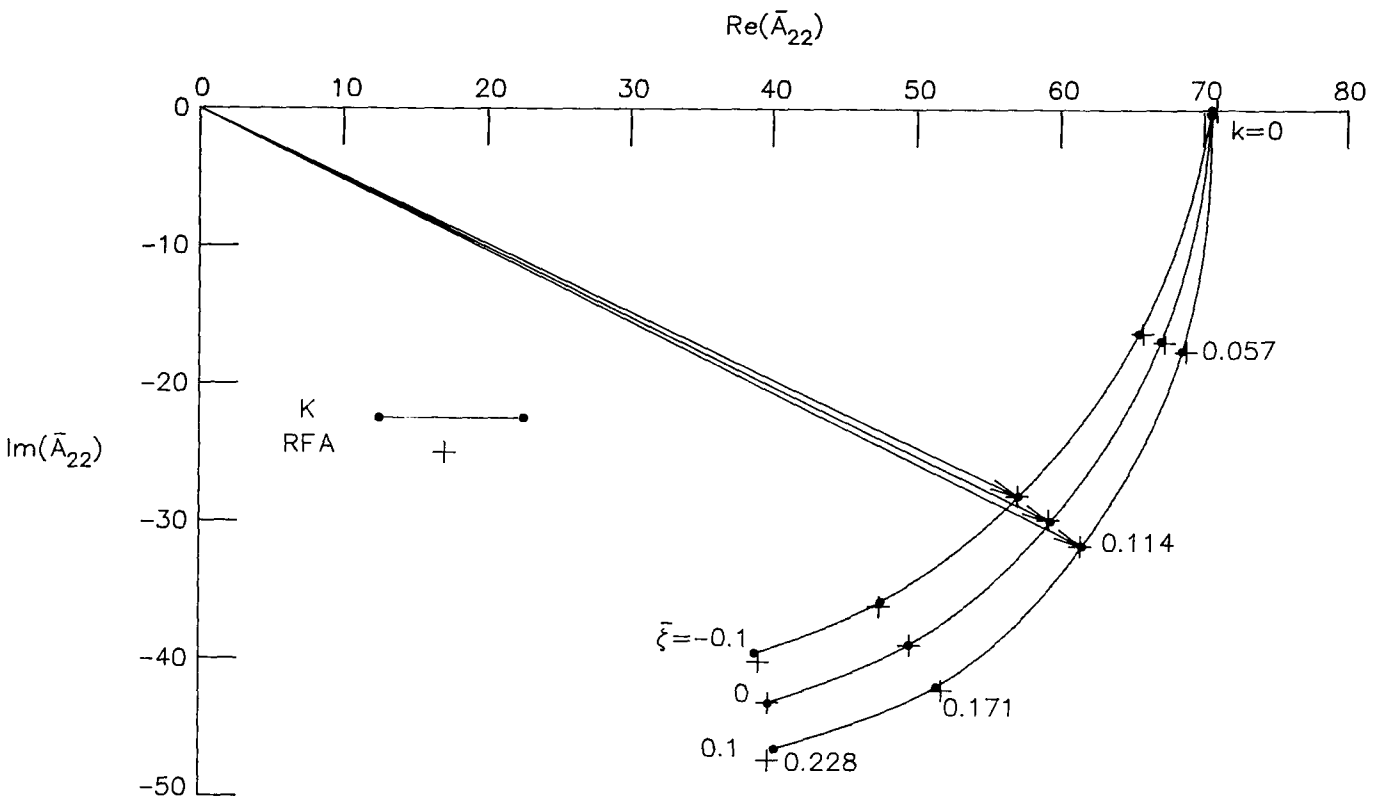

(a) $\bar{A}_{22}$.

Figure 4.- Generalized aerodynamic forces for growing and decaying motions of the four-percent-thick rectangular-planform flutter model of Doggett, Rainey, and Morgan (NASA TM X-79, 1959). $0 \leq k \leq 0.228$; $M = 0.904$.

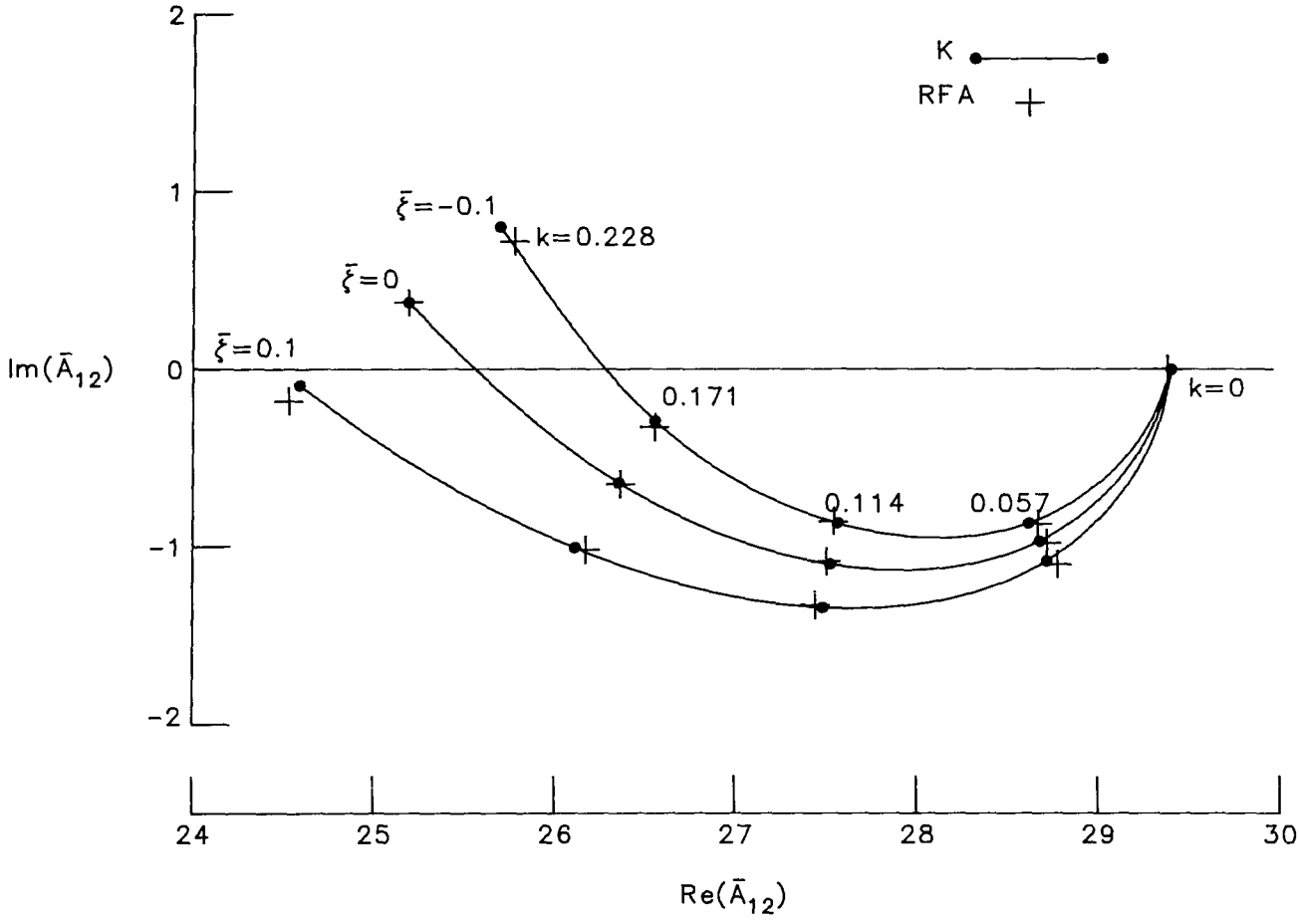

(b) $\bar{A}_{12}$.

Figure 4.- Concluded.

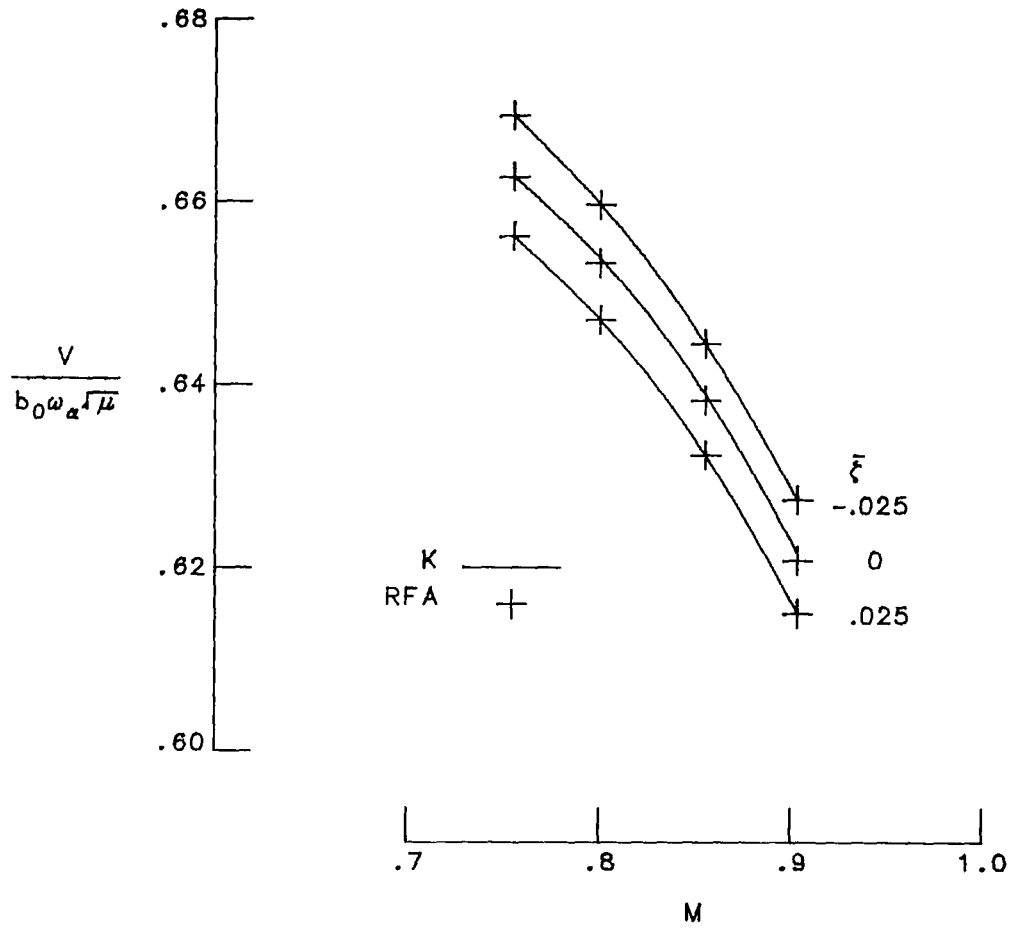

Figure 5.- Speed index versus Mach number for four-percent-thick rectangular-planform flutter model of Doggett, Rainey, and Morgan (NASA TM X-79, 1959).

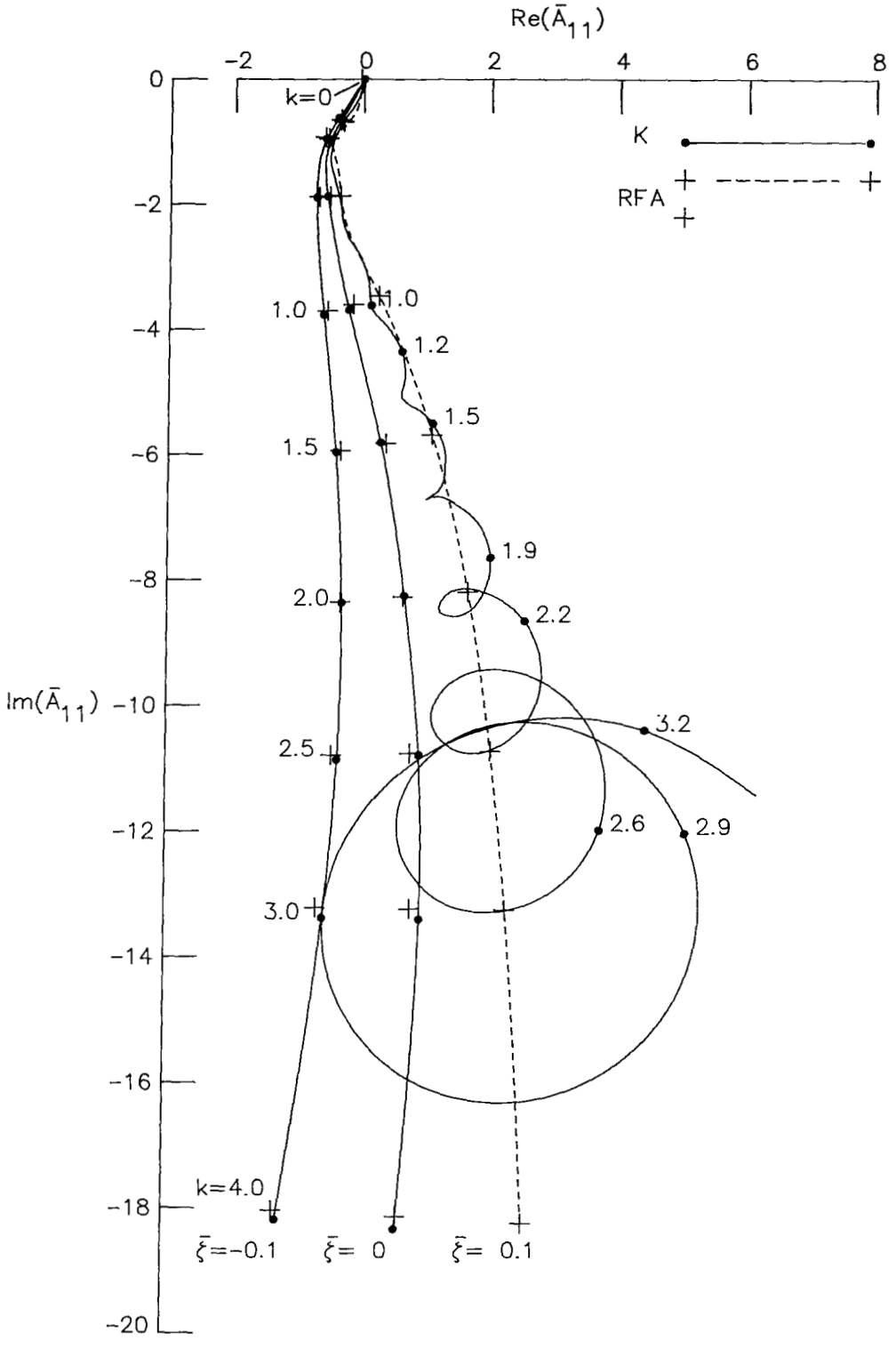

(a) $\bar{A}_{11}$, lift due to plunging oscillation. $0 \leq k \leq 4$.

Figure 6.- Generalized aerodynamic forces for growing and decaying motions of a two-dimensional airfoil section. M = 0.9.

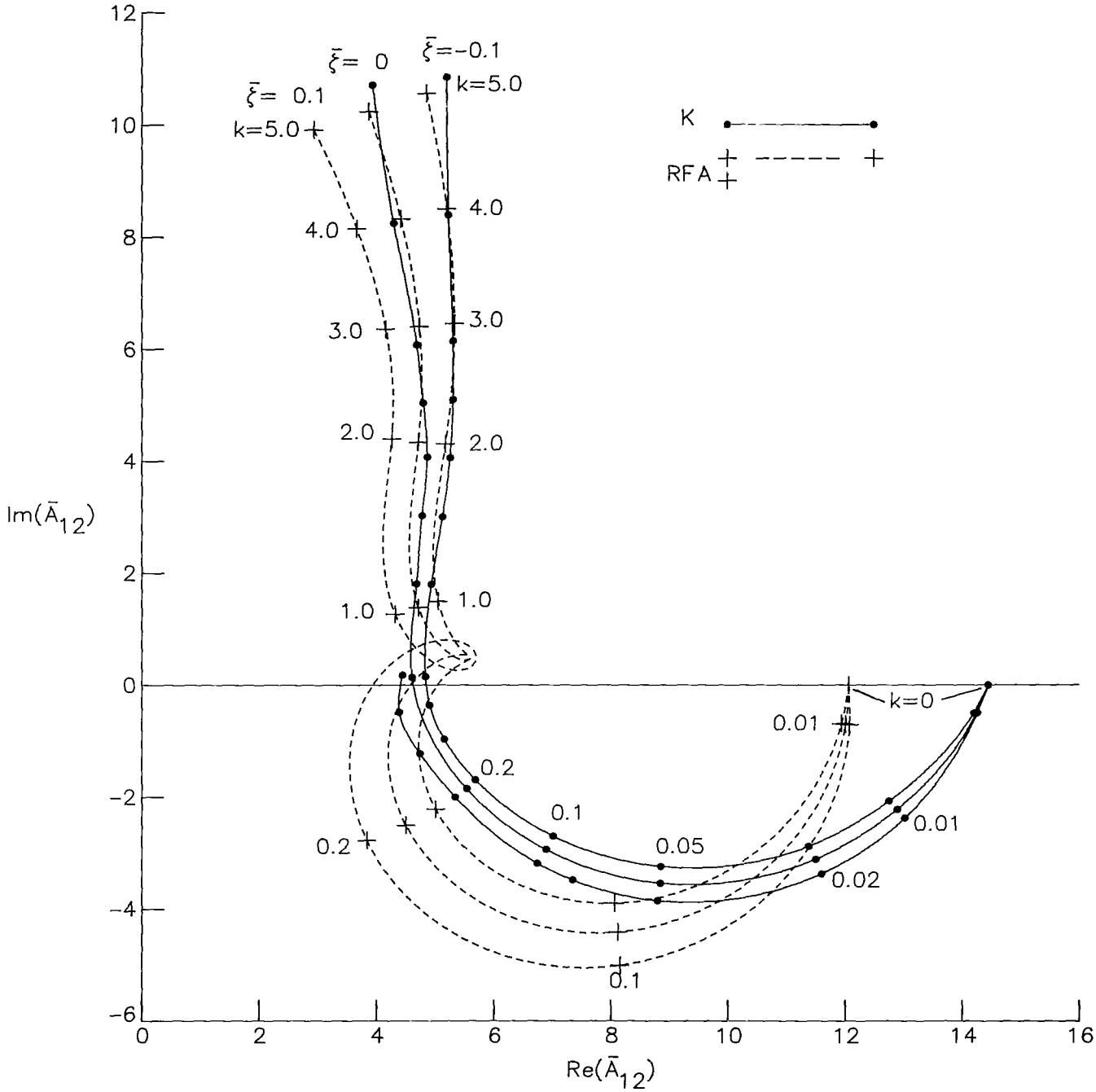

(b) $\bar{A}_{12}$, lift due to pitching at quarter-chord. $0 \leq k \leq 4$. (See detail on fig. 6(c).)

Figure 6.- Continued.

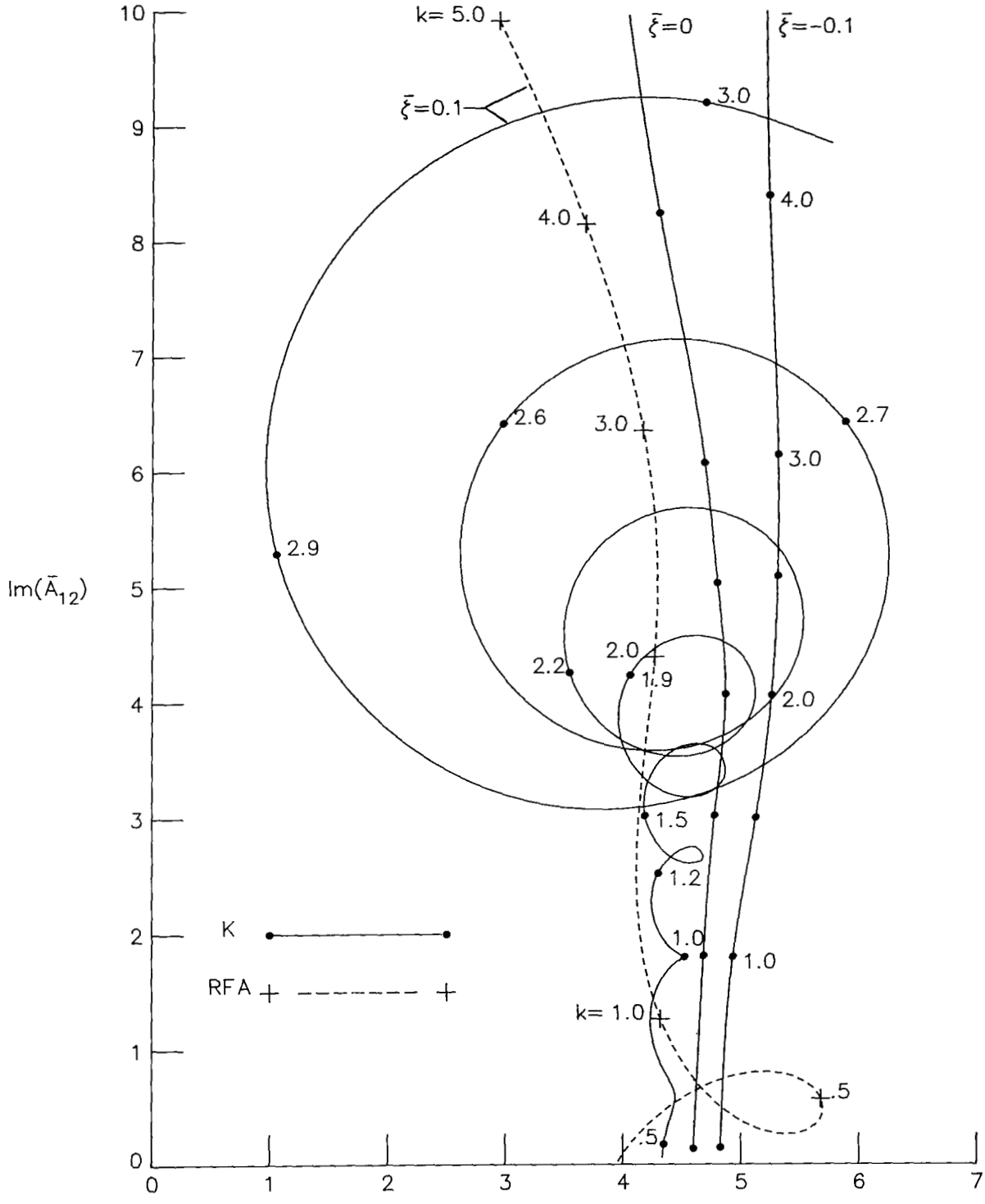

(c) $\bar{A}_{12}$ for $0.5 \leq k \leq 4.5$ with additional kernel-function results for $\bar{\zeta} = 0.1$.

Figure 6.- Concluded.

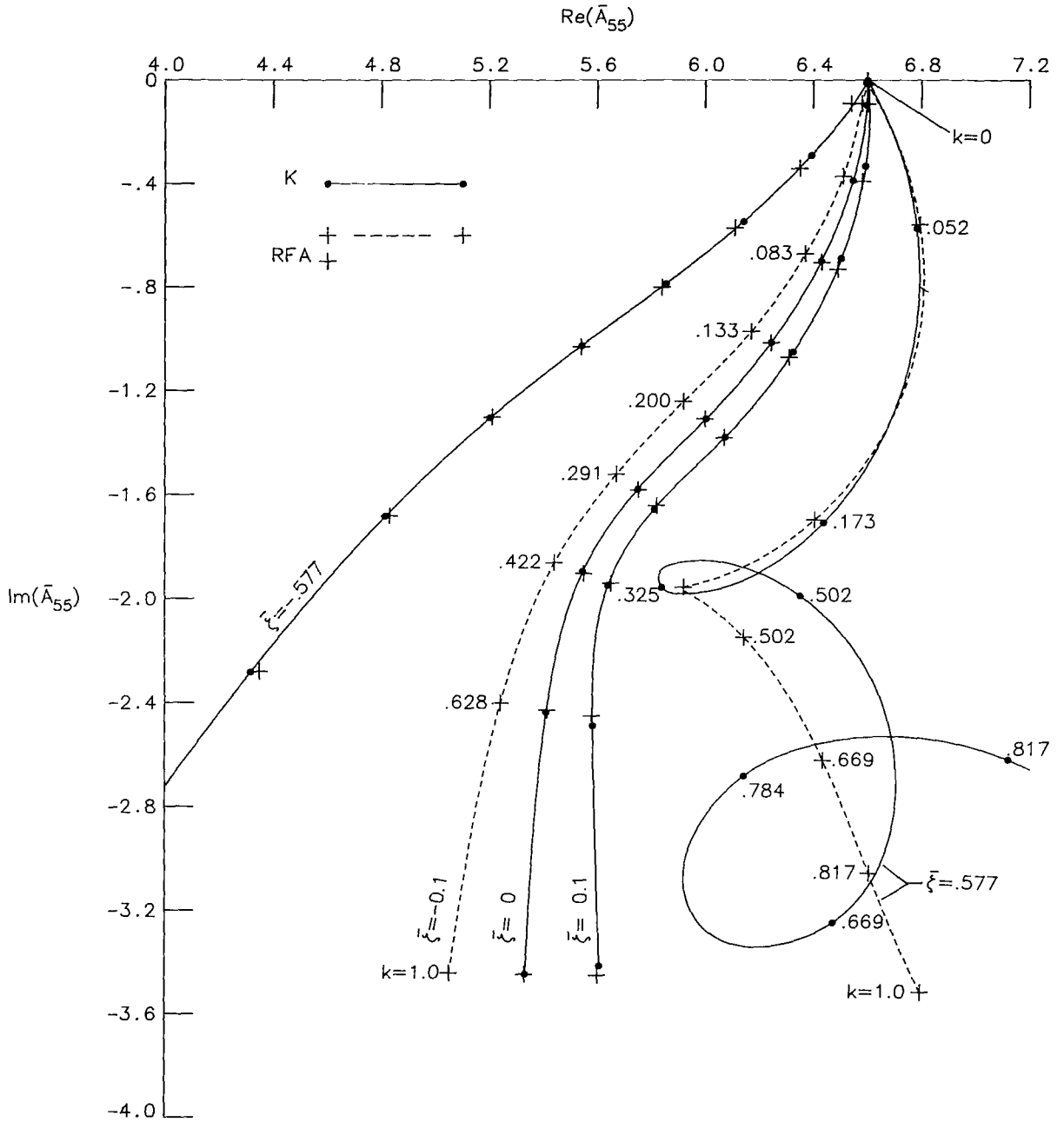

Figure 7.- Generalized force $\bar{A}_{55}$ for growing and decaying motions of the DAST ARW-1 wing. M = 0.8; $0 \leq k \leq 1.0$. Mode 5 is "first torsion."

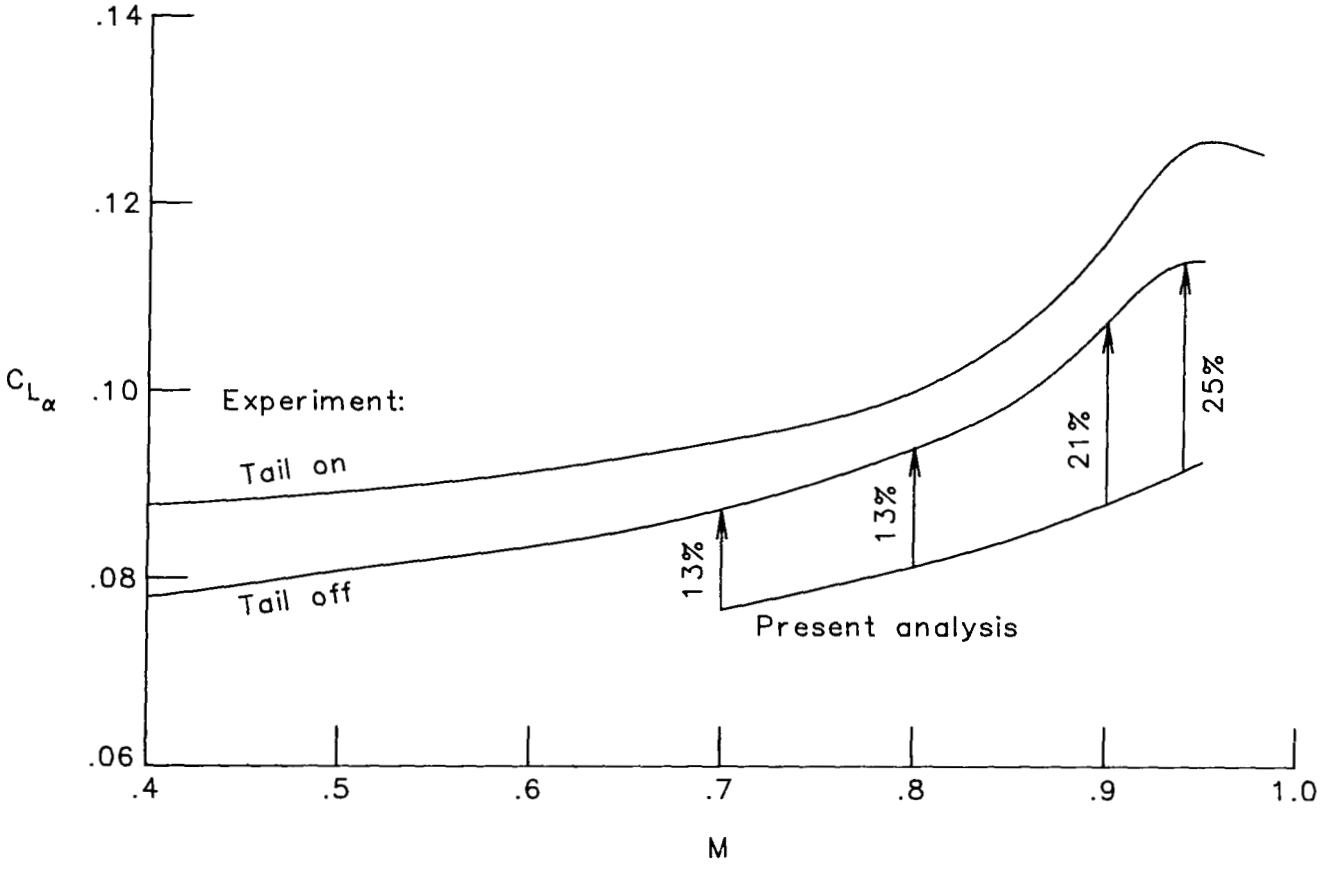

Figure 8.- Variation of lift-curve slope with Mach number. The two experimental curves are from Byrdsong and Hallissy (NASA TP-1360, 1979).

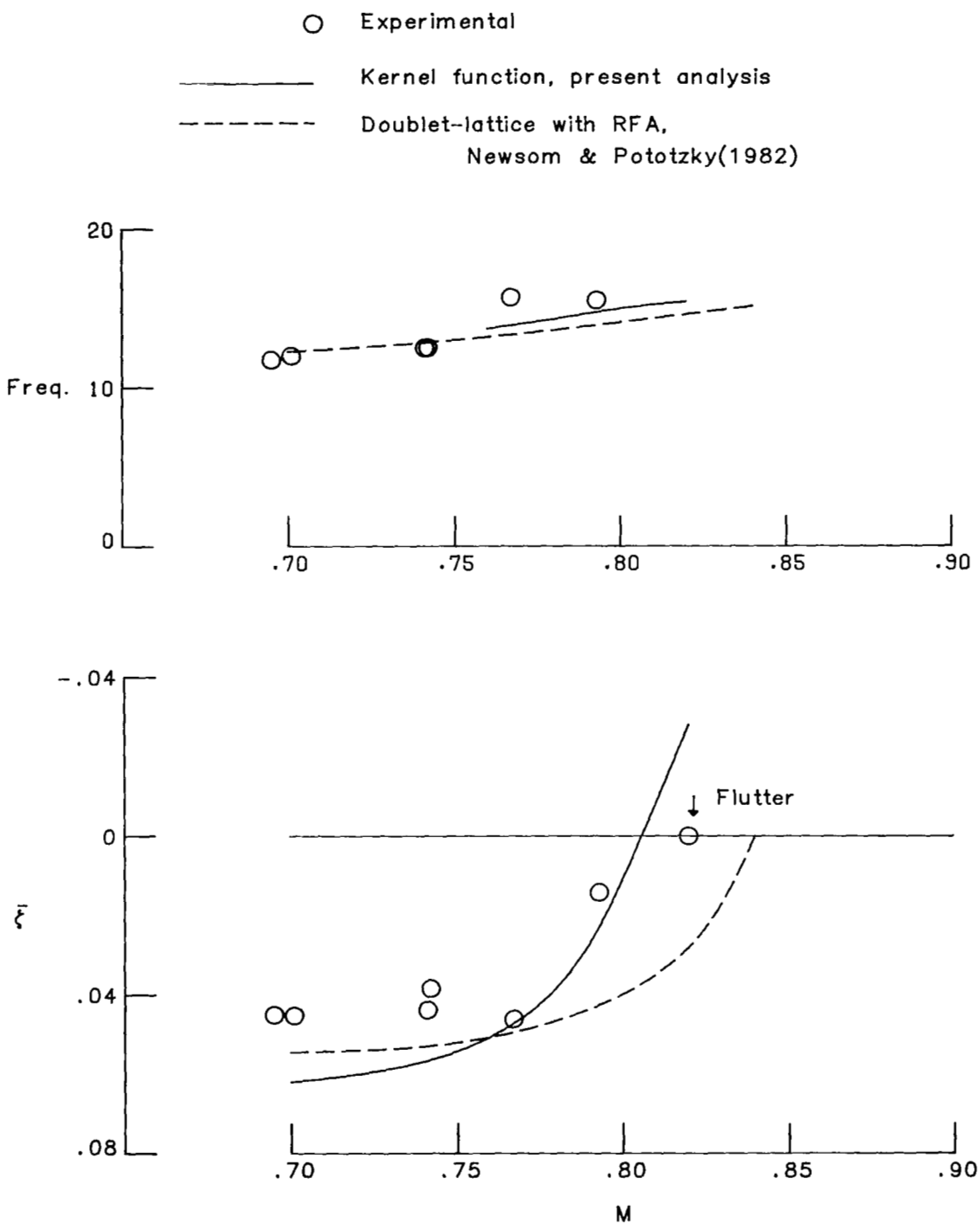

(a) Altitude = 15000 feet.

Figure 9.- Flutter-mode damping ratio and frequency versus Mach number for the DAST ARW-1 wing at two altitudes.

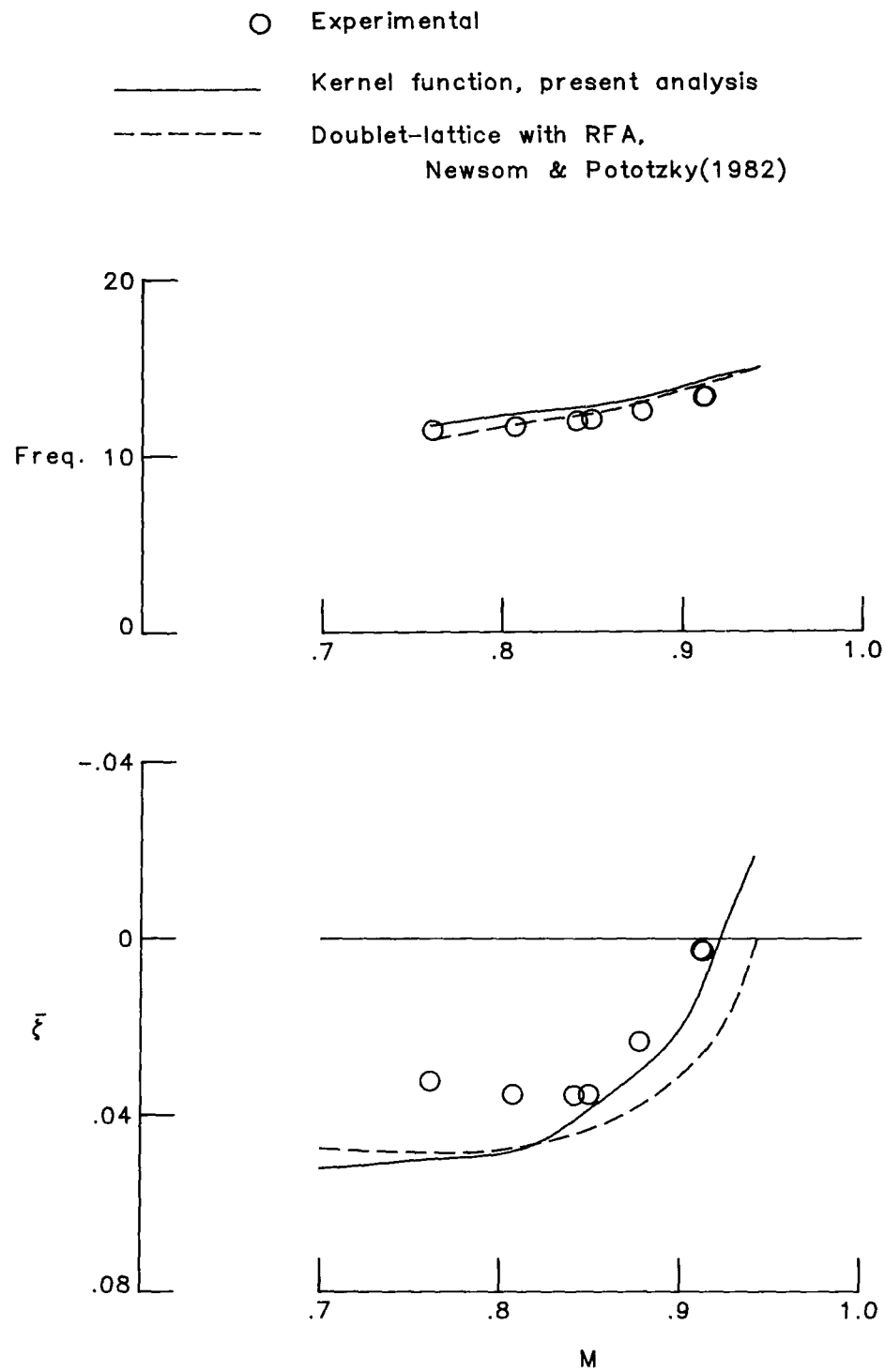

(b) Altitude = 25000 feet.

Figure 9.- Concluded.

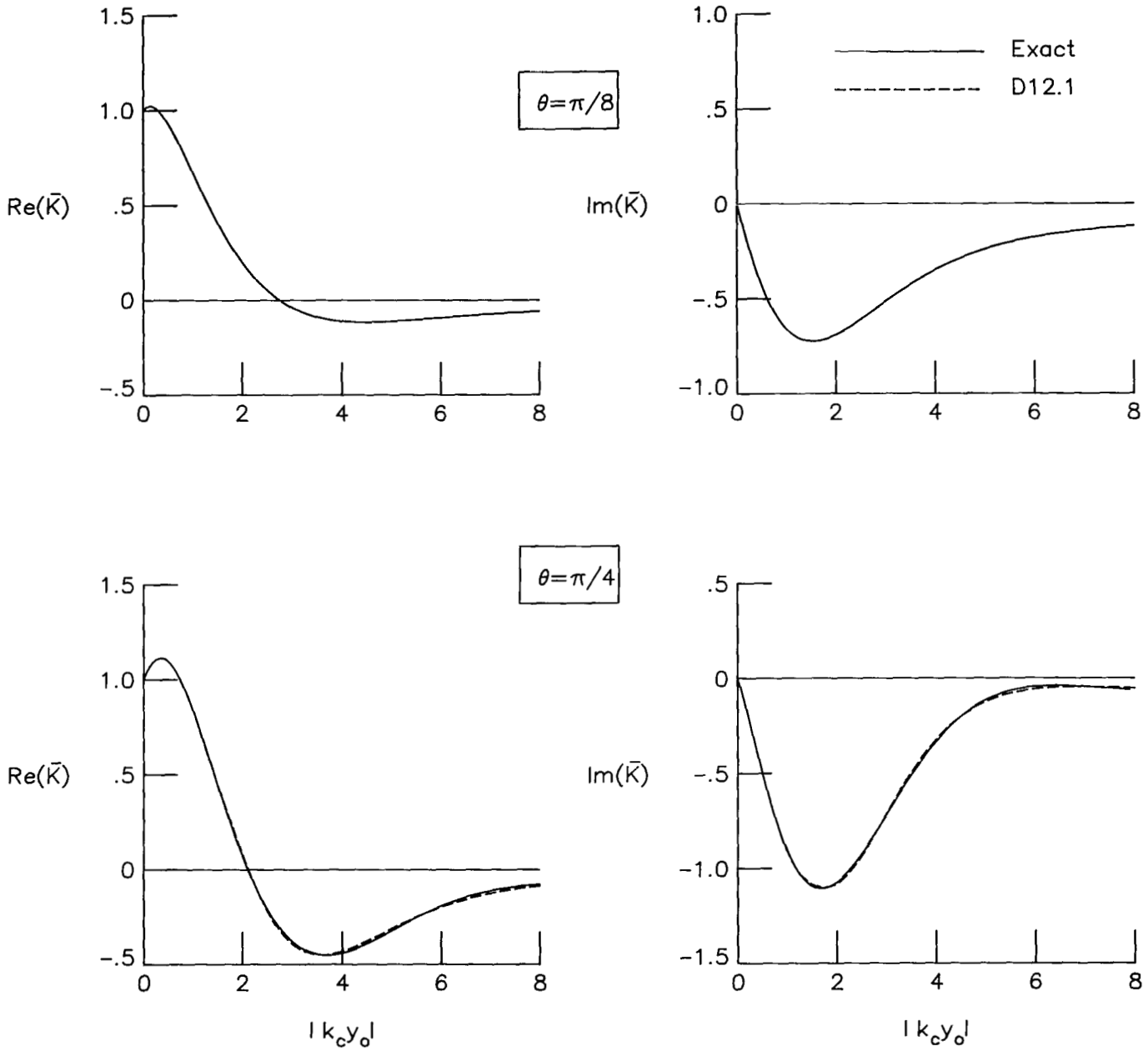

(a) Comparison with D12.1.

Figure 10.- Comparison of exact $\bar{K}$ with approximations D12.1 and L11 plotted as functions of $|k_c y_o|$ for two damping ratios denoted by θ.

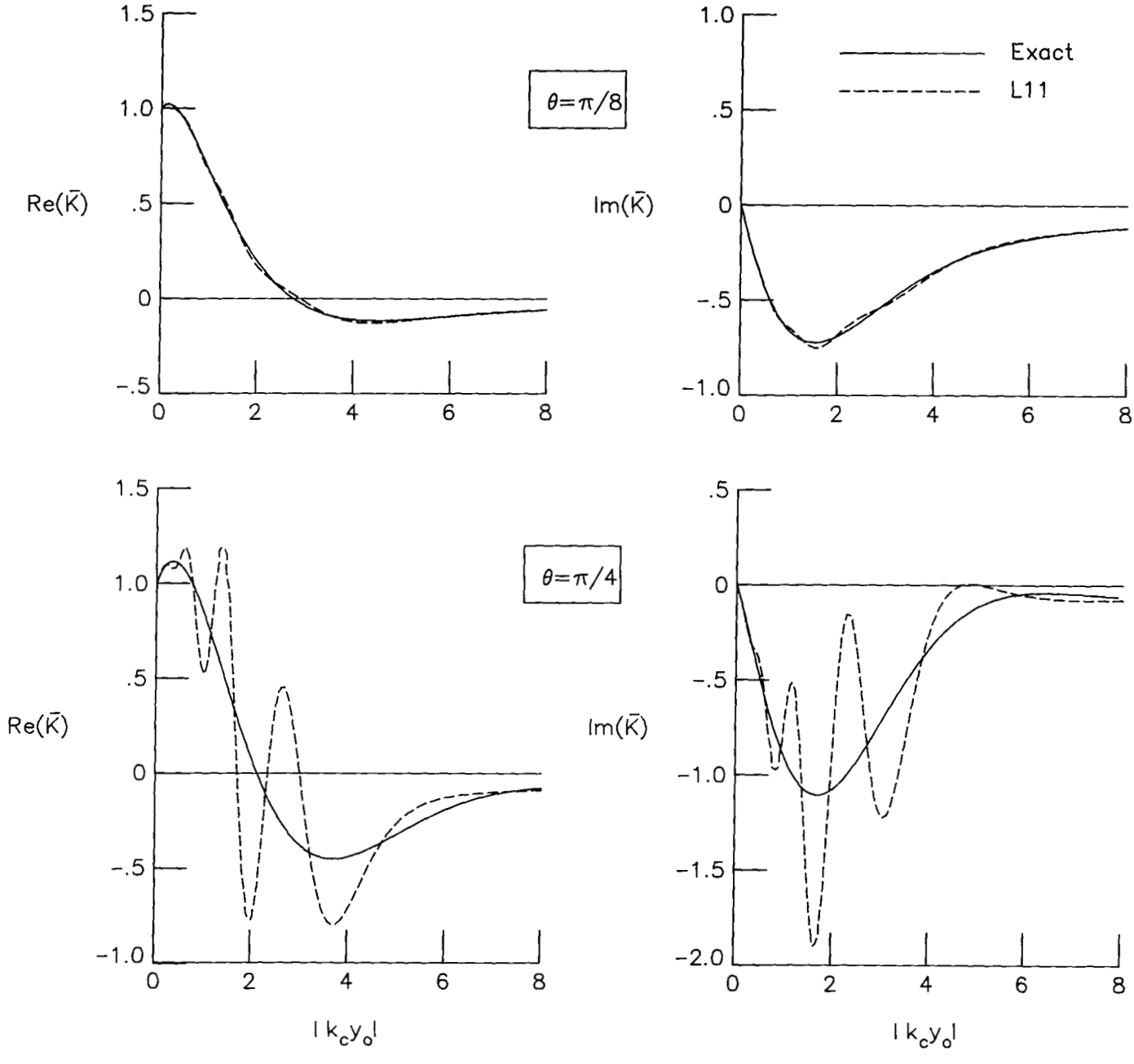

(b) Comparison with L11.

Figure 10.- Concluded.

1. Report No.	2. Government Accession No.	3. Recipient's Catalog No.
NASA TP-2292		

4. Title and Subtitle	5. Report Date
GENERALIZATION OF THE SUBSONIC KERNEL FUNCTION IN THE s-PLANE, WITH APPLICATIONS TO FLUTTER ANALYSIS	March 1984
	6. Performing Organization Code: 505-33-43-09
7. Author(s): Herbert J. Cunningham and Robert N. Desmarais	8. Performing Organization Report No.: L-15708
	10. Work Unit No.
9. Performing Organization Name and Address: NASA Langley Research Center, Hampton, VA 23665	11. Contract or Grant No.
	13. Type of Report and Period Covered: Technical Paper
12. Sponsoring Agency Name and Address: National Aeronautics and Space Administration, Washington, DC 20546	14. Sponsoring Agency Code

15. Supplementary Notes

16. Abstract

A generalized subsonic unsteady aerodynamic kernel function, valid for both growing and decaying oscillatory motions, is developed and applied in a modified flutter analysis computer program to solve for boundaries of constant damping ratio as well as the flutter boundary. Rates of change of damping ratios with respect to dynamic pressure near flutter are substantially lower from the generalized-kernel-function calculations than from the conventional velocity-damping (V-g) calculation. A rational function approximation for aerodynamic forces used in control theory for s-plane analysis gave rather good agreement with kernel-function results, except for strongly damped motion at combinations of high (subsonic) Mach number and reduced frequency.

17. Key Words (Suggested by Author(s)): Aerodynamic forces, Unsteady flow, Aeroelasticity, Control theory, Flutter, Kernel function

18. Distribution Statement: Unclassified - Unlimited

Subject Category 02

19. Security Classif. (of this report)	20. Security Classif. (of this page)	21. No. of Pages	22. Price
Unclassified	Unclassified	37	A03

For sale by the National Technical Information Service, Springfield, Virginia 22161

NASA-Langley, 1984

4 1 1U,A, 840315 S00903DS
DEPT OF THE AIR FORCE
AF WEAPONS LABORATORY
ATTN: TECHNICAL LIBRARY (SUL)
KIRTLAND AFB NM 87116

S